Evaluating Secondary Inorganic Aerosols in 3-Dimensions

Keren Mezuman[1,2], **Susanne E. Bauer**[3,2,*], **Kostas Tsigaridis**[3,2]
[1]Earth and Environmental Sciences, Columbia University, New York, NY, USA
[2] NASA Goddard Institute for Space Studies, New York, NY, USA
[3] Center for Climate Systems Research, Columbia University, New York, NY, USA
* To whom correspondence should be addressed, susanne.bauer@columbia.edu

Abstract.

The spatial distribution of aerosols and their chemical composition dictates whether aerosols have a cooling or a warming effect on the climate system. Hence, properly modeling the 3-dimensional distribution of aerosols is a crucial step for coherent climate simulations. Since surface measurement networks only give 2-D data, and most satellites supply integrated column information, it is thus important to integrate aircraft measurements in climate model evaluations. In this study, the vertical distribution of secondary inorganic aerosol (i.e. sulfate, ammonium and nitrate) is evaluated against a collection of 14 AMS flight campaigns and surface measurements from 2000-2010 in the USA and Europe. GISS ModelE2 is used with multiple aerosol microphysics (MATRIX, OMA) and thermodynamic (ISORROPIA II, EQSAM) configurations. Our results show that the MATRIX microphysical scheme improves the model performance for sulfate, but that there is a systematic underestimation of ammonium and nitrate over the USA and Europe in all model configurations. In terms of gaseous precursors, nitric acid concentrations are largely underestimated at the surface while overestimated in the higher levels of the model. Heterogeneous reactions on dust surfaces is an important sink for nitric acid, even high in the troposphere. At high altitudes, nitrate formation is calculated to be ammonia limited. The underestimation of ammonium and nitrate in polluted regions is most likely caused by a too simplified treatment of the NH_3/NH_4^+ partitioning which affects the

27 HNO_3/NO_3^- partitioning.

28 **1. Introduction**

29 The impact of aerosols on climate and air quality is a function of their chemical composition,
30 abundance and spatial distribution. Understanding the vertical profile of aerosols is crucial for
31 radiative forcing calculations (Xu and Penner, 2012), since aerosols interact with radiation
32 directly through absorption and scattering (Bauer and Menon, 2012; Haywood and Boucher,
33 2000; Stocker et al., 2013), and indirectly via interactions with clouds (Lohmann and Feichter,
34 2005). Comparisons of model results with organic aerosol aircraft data showed large
35 discrepancies in the free troposphere (Heald et al., 2005, 2011). Sulfate and ammonium nitrate
36 aerosols, although much simpler to model than organics, have not been studied in the vertical
37 in much detail. There is large uncertainty in the magnitude of the forcing induced by sulfate and
38 ammonium nitrate aerosols, with estimates for the preindustrial to present day direct radiative
39 forcing of sulfate ranging from -0.6 to -0.2 Wm^{-2} while for ammonium nitrate from -0.3 to -0.03
40 Wm^{-2} (Stocker et al., 2013) under present day conditions. These forcings are projected to
41 change in the future, driven by trends in precursor emissions. The projected increase in
42 agricultural ammonia emissions, which will result in greater availability of ammonia, contrasted
43 with the projected reductions in NO_x emissions, can lead to an increased relative contribution
44 of ammonium nitrate to the total secondary inorganic aerosol (SIA) abundance, due to the
45 strong projected decrease of sulfate aerosols (Hauglustaine et al., 2014; Hodas et al., 2014).
46 Yet, the effect of these changes on ammonium nitrate concentrations are still a matter of active
47 research: *Paulot et al.* [2016] showed increases in nitrate load in the free troposphere, while
48 surface concentrations decreased, and *Pusede et al.* [2016] showed changes in tropospheric

chemistry in western USA, with increased ammonium nitrate production during daytime rather than at night.

Thermodynamically, ammonia tends to neutralize sulfuric acid over the highly volatile nitric acid (Tagaris et al., 2007). The formation of fine-mode nitrate is a function of ammonia, sulfate availability and relative humidity (RH), since its precursor, nitric acid, condenses following thermodynamic equilibrium (Potukuchi and Wexler, 1995a, 1995b). Sulfuric acid and nitric acid also participate in heterogeneous uptake on dust particles, forming coarse sulfate and nitrate, a process that acts as a sink for the gas phase precursors (Bauer and Koch, 2005; Ravishankara, 1997).

In this paper we evaluate ammonium, nitrate and sulfate aerosols in the NASA GISS ModelE2 against surface and aircraft observations, extending what *Bauer et al.* [2007b] did for nitrate aerosol for the year 2000, by using new aerosol configurations that had been implemented in GISS ModelE2 since then, and a substantially extended record of SIA measurements, both from ground stations and various flight campaigns. To assess the model in terms of SIA surface distribution and vertical profiles, we evaluated the performance of three aerosol configurations, described in section 2.1.1, by comparing them against surface data measured over the USA and Europe during 2000-2010, and 14 flight campaigns, as described in section 2.2. We then study the climatology of the model against measurements, both at surface and at higher altitudes (sections 3.1-3.3), and explore the model uncertainties with the help of sensitivity experiments (section 3.4).

2. Experimental approach

2.1 Model description

The NASA GISS ModelE2 model (Schmidt et al., 2014) was run with interactive tropospheric (Shindell et al., 2001, 2003) and stratospheric chemistry (Shindell et al., 2006) and coupled with three different aerosol configurations, as described below. A horizontal resolution of 2° in latitude by 2.5° in longitude and a vertical resolution of 40 layers to 0.1 hPa was used. The simulation was nudged using 6 hourly National Centers for Environmental Prediction (NCEP) reanalysis data (Kalnay et al., 1996) for the horizontal wind component. Sea surface temperatures (SSTs) and sea ice cover were prescribed using the Met Office Hadley Center's sea ice and sea surface temperature data set (HadISST1) (Rayner et al., 2003).

The nitrate optical depth of GISS ModelE2 in the CMIP5 archive was found to be problematic, consistent with the findings of *Shindell et al.* [2013] for a likely too high nitrate load. The model was using the Henry value of ammonia instead of the effective Henry value, which resulted in large abundances of ammonia, hence ammonium, hence nitrate. In our work the nitrate scheme had been corrected and nitrate distribution in the column reflects surface sources such as agricultural, industrial and biomass burning areas.

2.1.1 Aerosols schemes

Two aerosol schemes were used in this study: OMA (One Moment Aerosol) (Koch et al., 2006; Miller et al., 2006) and MATRIX (Multiconfiguration Aerosol TRacker of mIXing state) (Bauer et al., 2008). OMA is a bulk mass scheme with one fine mode bin of prescribed size for SO_4^{2-}, NH_4^+, and NO_3^-. In OMA, heterogeneous uptake of SO_2 and HNO_3 on dust surfaces is also included, which takes place on the three smallest size bins out of the five size bins used for mineral dust (Bauer et al., 2004, 2007). This was changed after Bauer et al., 2007 where dust was

92 represented in four size classes, and coating on all classes was tracked. MATRIX is a
93 microphysical scheme representing nucleation, condensation and coagulation. Sulfate is
94 tracked with both number and mass concentrations for 16 populations, which are based on
95 mixing state. MATRIX represents an intermediate level of complexity; only the total mass of
96 nitrate, ammonium and aerosol water is calculated, and then distributed across populations
97 based on the sulfate abundance in each one of them, assuming internally mixed components.
98 This approach greatly reduces the required number of transported variables.
99 Due to the focus on SIA in this paper we will give a brief description of the sulfate and nitrate
100 schemes in our model. The sulfate chemistry module in both schemes, OMA and MATRIX, is
101 based on Koch et al. (1999) and includes prognostic calculation of gas and aqueous phase DMS,
102 MSA, SO_2 and sulfate concentrations. This provides the sulfate mass in the OMA scheme, and
103 provides aqueous sulfate production rates and H_2SO_4 concentrations as input parameters for
104 MATRIX microphysics (Bauer et al., 2008).
105 To partition between the gas and particle phases the model uses the non-linear
106 thermodynamics. Both schemes were run coupled to the secondary inorganic aerosol
107 thermodynamics scheme EQSAM (Metzger et al., 2002a, 2002b). MATRIX was also run coupled
108 to ISORROPIA II (Fountoukis and Nenes, 2007), which was only recently introduced into GISS
109 ModelE2. EQSAM is a parameterized thermodynamics scheme that relies on the relationship
110 between activity coefficients and RH to calculate the solute activity and the non-ideal solution
111 properties, while ISORROPIA II calculates the equilibrium constants and solves the
112 thermodynamic equations analytically. Both models use the same input parameters: NH_x
113 (NH_3+NH_4^+), SO_4^{2-}, XNO_3 (HNO_3+NO_3^-), RH and temperature, and interactively calculate the SO_4^{2-}

, NH_4^+, NO_3^- and aerosol H_2O concentrations at equilibrium, as well as the residual NH_3 and HNO_3 in the gas phase.

The thermodynamical equilibrium for Aitken mode sized particles, which is important for CCN, might not be properly captures by models (*Benduhn et al.* [2016]). This is not expected to be a problem in this study because Aitken mode particles are a small fraction of the total aerosol mass. In addition, for the coarse mode, large uncertainties exist regarding the availability of crustal and coarse mode material in equilibrium thermodynamic calculations. Our simulations do not take into consideration crustal (e.g. Mg^{2+}, K^+, Ca^{2+}) and sea salt (e.g. Na^+, Cl^-) ions in the thermodynamics, although this option is available in the model.

The model ran in the following three configurations: OMA-EQSAM, MATRIX-EQSAM, and MATRIX-ISORROPIA, and we are comparing model $PM_{2.5}$ (particles with dry diameter smaller than 2.5 μm) with measured $PM_{2.5}$ at surface, and model PM_1 (particles with dry diameter smaller than 1 μm) with measured PM_1 at the vertical, for consistency with the available measurements.

2.1.2 Emissions

This study used the Coupled Model Intercomparison Project phase 5 (CMIP5) historical anthropogenic emissions until 2005 (Lamarque et al., 2010) and the Representative Concentration Pathway 4.5 (RCP4.5) scenario thereafter (van Vuuren et al., 2011). Biomass burning emissions came from the Global Fire Emissions Database (GFED3) inventory (van der Werf et al., 2010). The emissions include seasonal variations for the biomass burning, soil NO_x, shipping and aircraft sectors (Lamarque et al., 2010), yet lack seasonal variability for all other anthropogenic emissions, including agricultural NH_3 sources. In order to prevent unrealistic

ammonium and nitrate aerosols loads during wintertime, the agricultural NH_3 emissions were altered using the local solar zenith angle, in order to produce a more realistic seasonal variability, but kept the total annual emissions the same. This approach is comparable to *Adams et al.* [1999] and *Park* [2004] who scaled ammonia emissions from crops and fertilizers according to the number of daylight hours.

2.1.3 Sensitivity runs

NH_3 emissions are controlled by the agricultural sector (Lamarque et al., 2010), both in the USA and Europe, where more than 80% of NH_3 emissions are agriculture-related (van Damme et al., 2015; Paulot et al., 2014). We test how changing agricultural NH_3 emissions affect ammonium nitrate formation under two scenarios: double and five times higher agricultural NH_3 emissions, using the MATRIX-ISORROPIA aerosol configuration. The results of that sensitivity are presented in section 3.4.

2.2 Observational datasets

2.2.1 Surface measurements

We evaluate our simulations against nitrate and sulfate $PM_{2.5}$ data measured by the Interagency Monitoring of Protected Visual Environments (IMPROVE) network over the continental United States (Malm et al., 1994, 2004), and against ammonia, ammonium, nitric acid, nitrate, SO_2 and sulfate measured by the European Monitoring and Evaluation Programme (EMEP), available via the NILU-EBAS database, for the years 2000-2010. From EMEP we use the corrected sulfate for sea salt (XSO_4) (EMEP, 2014, Chp. 3) as it better represents fine sulfate. IMPROVE currently has 212 sites, predominantly rural (Hand et al., 2011, 2012), while EMEP has

around 40 sites measuring aerosol composition in Europe, many of which are urban (Tørseth et al., 2012). The data in Europe is reported in μgX m^{-3} (where X is either sulfur or nitrogen) and in the USA in μg m^{-3}. We decided to keep these units unchanged in the rest of the manuscript, and convert the units of the model to represent those of the measurements, rather than doing the opposite. We compared monthly mean values from all available stations with monthly mean model output. An examination of the mean spatial distribution over the USA (Figure 1) revealed distinct regimes with different pollution levels, which motivated a regional division of the data into eastern USA (EUSA) and western USA (WUSA). Europe (EU; Figure 2) and the Arctic (ARC; data from flight campaigns only) were studied independently (Table 1). The standard deviation, correlation coefficient (R), and normalized mean bias (NMB) between the monthly mean surface values within the studied regions (black frames in Figures 1 and 2) and the model's monthly mean at the stations locations in each region, were calculated. It is important to note that during the 11-year period the number of measuring sites has varied in each region, and that not all stations measured all species.

2.2.2 Flight campaigns

The Aerodyne Aerosol Mass Spectrometer (AMS), which measures chemical composition and size distribution of non-refractory particles (such as ammonium, nitrate and sulfate) with diameter smaller than 1 μm (Allan et al., 2003; Jimenez et al., 2003), had been part of many flight campaigns in the past decade. Another common method to measure inorganic particle composition is using the particle-into-liquid-sampler (PILS), which quantifies the ionic content of particulate matter using ion chromatography (Weber et al., 2001). In this study we use data from 14 flight campaigns, two of which used the PILS instrument for chemical composition

179 measurements, and the rest used the AMS (Table 2). The flights took place in the Northern
180 Hemisphere during short campaign periods, predominantly during spring and summer seasons,
181 between 2001-2011. The flight tracks of the campaigns used here are presented in Figure 3.
182 Data were retrieved using the Tools for Airborne Data interface (https://tad.larc.nasa.gov/), as
183 well as the AMS global database (https://sites.google.com/site/amsglobaldatabase/). For every
184 campaign a mean regional vertical profile was calculated by averaging the flight data within the
185 model's grid. For short-range campaigns such as ACE, CRISTAL, MILAGRO, TexAQS, and EUCAARI
186 all available data were used, for ITOP the transit flight data were parsed out, and for the rest of
187 the campaigns only data within the regional boundaries we study (black frames in Figure 3)
188 were used. These boundaries were chosen in accordance with the surface observations.
189 The campaign-average profile was compared against the monthly mean model output, a not
190 uncommon practice in model-aircraft comparison studies (e.g. Bauer et al., 2007; Emmons et
191 al., 2000; Shindell et al., 2003). The simulations were sub-sampled by taking into consideration
192 the geographical variability of the flights, but not the sub-monthly temporal variability, to yield
193 a mean corresponding profile. The one standard deviation variability of the campaign data per
194 model level was calculated for the measurements and model simulations, which represents the
195 spatial variability of the concentrations during the whole field campaign for the measurements,
196 and the spatial variability of the monthly mean modeled concentrations for the model. The
197 duration of the field campaigns ranged from 7 to 17 days. In the Results section we picked 4
198 representative campaigns that display systematic behavior, one for each region (Figure 7). The
199 rest of the campaigns can be found in the appendix (Figure A2, A3).

200 **3. Results and discussion**

In terms of mean surface concentrations (measured and modeled) in the Western Hemisphere sulfate concentrations are higher than nitrate concentrations. That is not the case in the Eastern Hemisphere, since over western Europe sulfate and nitrate aerosols are comparable in mass (Figure 2), consistent with *Schaap et al.* [2004]. At the whole atmospheric column (not shown here), sulfate peaks over east EU and northern Africa due to in-cloud production and transport, while the nitrate column distribution corresponds to the surface distribution, with maxima over the continental hot spots, driven by urban pollution and biomass burning.

3.1 Surface climatology

Surface data show high concentrations of nitrate and sulfate in the industrialized EUSA and EU and lower concentrations in WUSA, with some urban hot spots (Figures 1 and 2). We compared the model skill, with respect to measurements, under the three different aerosol configurations in Figure 4 for nitrate (left) and sulfate (right). The regional clusters observed reflect the fact that performance in terms of R and NMB is controlled by region rather than aerosol scheme. For sulfate, the simulation with no microphysics (OMA, blue) is always biased lower (by 1-4%) compared to the other two simulations (MATRIX, red and green). This result is due to the microphysical processes included in MATRIX (i.e. nucleation, condensation and coagulation), which allow for aerosols to spread over the entire size distribution, including the existence of smaller particles (the freshly nucleated ones), which sediment more slowly. Additionally the solubility of sulfate in MATRIX is calculated as a weighted average of the mixed particle component's solubility (SO_4 mixed with dust, BC, etc.), and is always less than the pure SO_4 solubility in OMA. The differences in both size and solubility lead to a longer lifetime of MATRIX sulfate, thus increasing the aerosol mass. As an indication, the mean lifetime of sulfate in 2005

was 4.2 days in the two MATRIX simulations, against 3.2 days in the OMA simulation. We observe a systematic underestimation of ammonium, nitrate and sulfate in EUSA and EU (35% for nitrate, 30% for ammonium, 20% for sulfate). Despite the negative bias, the three aerosol types correlate well with measurements in these regions (R>0.5). This high correlation is due to the fact the simulations successfully capture the aerosol seasonal cycle (discussed in the next section). In the WUSA, the simulations overestimate sulfate by 12%, and underestimated nitrate by 80%, while there is no correlation between the model and observations for nitrate. The different behavior across regions reflects the fact that the WUSA is driven by agricultural emissions while in the EUSA industrial and residential emissions dominate. The ability of the model to capture the seasonality (discussed in the next section) is important for model skill and is discussed in the next section.

3.2 Surface seasonality

Figure 5 shows that in the EU there is little variation in the SO_2 seasonality between the three simulations, which is emission-level driven. The modeled surface concentration overestimates measurements by about 0.5 μgS m^{-3}, with an amplified seasonal cycle. Past studies (Dentener et al., 2006; Vestreng et al., 2007) have raised concerns regarding the accuracy of SO_2 emission inventories, which might be part of the explanation of the SO_2 overestimation. Additionally, wintertime chemistry slowdown due to reduced photochemistry increases the SO_2 lifetime, resulting in reduced sulfate formation rates, contributing to the underestimation of sulfate concentration which can be as high as a factor of 2 during winter months. For sulfate, the difference between the simulations is dominated by the aerosol scheme, with the summertime peak being more pronounced in the MATRIX simulations than in the OMA one. As explained in

245 the previous section, MATRIX simulates higher concentrations due to the existence of smaller
246 particles with longer lifetimes compared to OMA. Surface NH_3 (Figure 5) is overestimated in all
247 three simulations, which might be due to incorrect NH_x partitioning calculated by EQSAM and
248 ISORROPIA II, a hypothesis that is supported by the underestimate of ammonium. Contrary to
249 SO_2 and NH_3, nitric acid is underestimated by the simulations by a factor of 3. This contributes
250 to the underestimation of nitrate in all simulations**.** The simulated seasonality of nitrate
251 matches that of the measurements, peaking during winter and reaching a minimum during
252 summer. *Konovalov et al.* [2008] identified a slight underestimation of NO_x in emission
253 inventories in southern Europe, which would contribute to underestimations of XNO_3.
254 IMPROVE has extensive sulfate and nitrate surface data to compare against the model
255 simulations. EMEP provides additional HNO_3 data from 9 stations, predominantly around the
256 Great Lakes, which is not enough for a proper regional analysis. Unfortunately, ammonium and
257 gas phase aerosol precursors are not routinely measured via the IMPROVE network. In the
258 eastern USA (Figure 6) the model simulations exhibit peak sulfate concentrations during
259 summer, with the MATRIX simulations having a stronger seasonality than OMA, which better
260 matches observations. For nitrate, all simulations systematically underestimate measurements
261 during most of the year (by about 0.2 $\mu g\ m^{-3}$), except during winter, where MATRIX slightly
262 overestimates them (less then 0.1 $\mu g\ m^{-3}$). The HNO_3 underestimation by the model, as evident
263 by the limited measurements we obtained in EUSA (Figure A1), contributes to the nitrate
264 underestimation.
265 In WUSA the simulated sulfate and nitrate seasonality (Figure 6 left panels) is flat compared to
266 the measurements. For sulfate, the measured range is 0.7 $\mu g\ m^{-3}$, while in the MATRIX

267 simulations the range is 0.25 μg m^{-3} and OMA-EQSAM is 0.15 μg m^{-3}. All simulations
268 underestimate measurements during summer and overestimate them during winter. The
269 measured maximum sulfate concentrations are around summer. This feature is captured by
270 OMA-EQSAM, but the MATRIX simulations calculate spring and fall peaks instead. For nitrate,
271 the measurements peak in early winter, a feature that is not captured by the simulations, as
272 modeled nitrate peaks in winter. During the winter OMA-EQSAM and MATRIX EQSAM are
273 similar, probably due to the common thermodynamical scheme, while MATRIX-ISORROPIA II is
274 higher by 0.05 μg m^{-3}. Modeled nitrate is underestimated compared to measurements
275 throughout the year: in the MATRIX simulations it is underestimated by about 0.45 μg m^{-3} (80%
276 of the measured value), and in OMA-ISORROPIA it is underestimated by about 0.4 μg m^{-3}.

277 **3.3 Vertical Profiles**

278 The simulated mean vertical profiles of sulfate, ammonium, nitric acid (when available), and
279 nitrate are evaluated against the mean measured profiles in Figure 7. The measured and
280 modeled standard deviations (gray shading and dashed lines, respectively), along with the
281 number of days each layer was sampled (black squares), are shown as well. Generally, aerosol
282 concentrations decrease with altitude as they peak near emission sources at the surface. Some
283 of the data used in this study were affected by intense fire plumes (Fisher et al., 2010; Jacob et
284 al., 2010), as can be seen in the ATCPAC (ARC) and ARCTAS spring and summer (ARC) panels
285 (Figure 7 and A2). Fires act as a source of NO_x, NH_3 and SO_2, increasing the concentration of
286 sulfate, ammonium and nitrate in the measurements. Fire emissions are included in our
287 simulations, yet these emissions could be underestimated, as *Ichoku and Ellison* [2014]

indicated is the case in many bottom-up emission inventories such as GFED3 (used here), and are also a function of properly resolving the transport. Even if all these factors are accurate in the model, the monthly mean output we use would dilute the signal of a fire event as observed in a flight profile.

Modeled sulfate concentrations are underestimated compared to the measurements (first column in Figure 7 and Figures A2 and A3). The MATRIX simulations that include aerosol microphysics show higher concentrations compared to the bulk scheme. During INTEX-A (EUSA) the MATRIX simulations produced in the boundary layer around 1 μg m^{-3} higher sulfate concentrations compared to OMA. The thermodynamic scheme (EQSAM or ISORROPIA II) makes a minor difference for sulfate, stemming from the simulations' climate feedbacks, with the green and red lines overlaying each other. All these results are consistent with the ones presented earlier for the surface.

In remote environments like the Florida Keys (CRISTAL-FACE, Figure A3), Azores (ITOP-UK, Figure A3) and the Arctic (ARCTAS spring and summer, Figure 7 and A2), ammonium and nitrate concentrations are generally very low, and the models are able to reproduce the aerosol concentrations. However, in campaigns over land such as: EUCAARI EU, EUSA: INTEX-A, NEAQS, DISCOVER-MD, CALNEX WUSA, TexAQS, and Mexico: MILAGRO-MIRAGE, INTEX-B, there is consistent underestimation of both ammonium and nitrate, especially in the boundary layer (Figures 7, A2 and A3). The sensitivity runs we performed, presented later, explore whether this is due to precursor levels or to the thermodynamic parameterization used.

From the nitric acid profiles (third column in Figure 7 and Figure A2), it is evident that the model strongly overestimates the measurements in the middle and upper troposphere. HNO_3 overestimation at high altitudes is consistent with Figure 10 from *Shindell et al.* [2006]. On top of that, the modeled nitric acid shows distinct OMA and MATRIX profiles, which diverge with increasing height, with differences that can become as high as 0.3 ppbv. Though there is not much dust at these altitudes, the inclusion of heterogeneous reactions on dust surfaces in OMA is the main difference in the gas phase chemistry of OMA and MATRIX schemes. The coarse mode nitrate mass formed by those heterogeneous reactions almost fully accounts for the difference in HNO_3 between the two schemes. However, this loss is insufficient to explain the discrepancy between the model and measurements. We exclude the nitrate that forms on dust (coarse nitrate) from the nitrate profiles, since neither they are in the PM_1 aerosol measurements, nor they are calculated in the MATRIX simulations.

The overestimation of nitric acid does not result in overestimation of nitrate, which is also affected by the availability of both sulfate and ammonia, on top of environmental factors like relative humidity and temperature. Even though nitrate concentrations are low in many locations (below 2 $\mu g\ m^{-3}$), the simulations underestimates it to be below 0.1 $\mu g\ m^{-3}$ in EUSA (INTEX-A in Figure 7, NEAQS, DISCOVER-MD, and TexAQS in Figure A2), WUSA (CALNEX in Figure 7), arctic (ARCPAC in Figure A2), Central America (INTEX-B in Figure A2, MILAGRO-MIRAGE, and CRISTAL-FACE in Figure A3), consistent with the spring-summer surface underestimation. Another key point is that there is little difference in the nitrate concentrations simulated by the different aerosol configurations. Differences between the simulations are evident only in the boundary layer in EUCAARI (EU, Figure 7), ~0.8 $\mu g\ m^{-3}$, and ACE-ASIA (Japan, Figure A3), ~0.3 μg

330 m^{-3}. In these locations, the difference is not evident on a thermodynamic scheme basis, but
331 rather on a microphysical scheme, with MATRIX-EQSAM and MATRIX-ISORROPIA grouped
332 against OMA-EQSAM. The difference in concentration between the simulations is also evident
333 in the ammonium profiles of these campaigns. In EUCAARI, nitrate and ammonium have higher
334 concentrations in the OMA-EQSAM simulation, while sulfate is consistently larger in the
335 MATRIX ones. In ACE-ASIA however, both sulfate and ammonium concentrations are higher
336 with OMA-EQSAM, yet nitrate concentrations are higher in the MATRIX simulations. It is
337 evident from these profiles that the simulations with lower sulfate concentrations are also the
338 simulations with higher nitrate concentrations. The role of thermodynamics to the NH_3/NH_4^+
339 partitioning at different NH_3 levels will be discussed in the next section.

340 **3.4 Sensitivity runs**

341 In order to study the interplay between precursor concentrations and thermodynamics we
342 perturbed the ammonia emissions from agriculture. For these runs, presented in Figure 8, we
343 use the MATRIX-ISORROPIA scheme with standard NH_3 emission (green line), double
344 agricultural NH_3 emissions (purple line) and five times agricultural NH_3 emissions (brown line).
345 At the surface, as NH_3 emissions are increased, the ammonium and nitrate underestimation by
346 the model disappears (Figure 8). However, a comparison with the limited available surface NH_3
347 measurements reveals that even with the standard NH_3 emissions the model overestimates
348 NH_3 concentrations. This is also evident in TexAQS and CALNEX (WUSA) NH_3 profiles (Figure A4).
349 Similarly, in the vertical, with increasing NH_3 emissions the nitric acid model overestimation
350 decreases (Figure A5), as more NH_3 becomes available to react with nitric acid and partition it

to the aerosol phase. These results indicate that the NH_3/NH_4^+ partitioning is not accurately calculated by the model, and that this strongly affects the nitric acid/nitrate partitioning. Further evidence to support our conclusion lies in Figure 9 that presents the modeled and measured partitioning ratios (NH_3 over total NH_x, and HNO_3 over total XNO_3). For NH_x all three simulations are grouped together, while for XNO_3 a distinct difference between the thermodynamic schemes is revealed: MATRIX-EQSAM overestimate the partitioning ratio during the summer, and MATRIX-ISORROPIA II is closer to measurements. From the surface seasonality of the individual species (Figure 5) it is clear that the divergence in the ratio is driven mainly by nitrate concentrations, as HNO_3 concentrations are the same for MATRIX-EQSAM and MATRIX-ISORROPIA II (red and green curves overlaying each other). The difference between these two simulations in terms of nitrate concentrations are of the order of 0.05 μg N m^{-3} and are most distinct during summer (Figure 5). Similarly, the difference between the simulations for XNO_3 is greater during summer. Thermodynamically, other than precursor levels, the difference in behavior in summer and the rest of the year is also controlled by temperature and RH.

Conclusions

In this work we used a collection of surface measurements and flight campaigns over the USA and Europe from 2000-2010 to study the regional and vertical distribution of secondary inorganic aerosols and their precursors under different aerosol configurations of the GISS ModelE2. In the USA sulfate aerosol dominate the near surface SIA composition, but over EU the nitrate aerosol contribution is comparable in mass.

372 We compare the behavior of SIA concentrations in high (EUSA, EU) and low (WUSA) aerosol
373 precursor source regions, as the relative contribution of different sectors generates different
374 chemical regimes. We observe a systematic underestimation of near surface concentrations in
375 the EUSA and EU compared to the surface network measurements: 35% for nitrate, 30% for
376 ammonium, 20% for sulfate. However, despite the negative bias, all three simulations have high
377 correlation coefficients (R>0.5) when compared against surface data. In the WUSA the results
378 for sulfate and nitrate are different in sign, sulfate is biased high (12%) with R=0.43, while
379 nitrate is biased low (80%) with no correlation between the simulations and the measurements
380 (R<0.1). The correlation is also driven by the difficulty of the model to capture the annual cycle
381 of the species.

382 Microphysics has improved the sulfate simulation, as the MATRIX scheme yields consistently,
383 both at the surface and in the vertical, higher sulfate concentrations, due to smaller particles
384 having longer lifetimes compared to OMA, the bulk scheme (4.2 days against 3.2 days). For
385 ammonium nitrate simulations there is an additional level of complexity in the form of accurate
386 thermodynamics, which is sensitive both to the precursors and to environmental parameters
387 such as temperature and humidity. Since we have performed nudged simulations, they do not
388 show big differences in temperature and RH, so the differences between the simulations are
389 expected to be dominated by the thermodynamical scheme and not the underlying
390 meteorological parameters. In terms of precursors, NH_3 is slightly overestimated, as indicated
391 by surface measurements over EU in Figure 5 and TexAQS and CALNEX campaigns in Figure A3.
392 HNO_3 is underestimated at the surface but overestimated at higher levels, and including
393 heterogeneous reactions on dust surfaces decreases the overestimation. A more complex

394 version of MATRIX, that currently does not exist, should include heterogeneous uptake on dust.
395 Overall, aerosol mass is consistently underestimated both at surface and in the boundary layer.

396 In our sensitivity runs, increasing NH_3 emissions results in NH_3 overestimation, however it
397 improves our simulated HNO_3 profiles. When more NH_3 is available it reacts with HNO_3 to form
398 ammonium nitrate, resolving underestimations in the aerosol phase. Hence, the partitioning of
399 NH_x which strongly affects the partitioning of XNO_3 is not accurately simulated in the model.
400 *Aan de Brugh et al.* [2012] identified an overestimation of gas phase precursors during daytime
401 (equivalent to summer) and overestimation of aerosol phase species during nighttime
402 (equivalent to winter), and found it to be related to the time scale of vertical mixing against the
403 timescale of thermodynamic equilibrium. This relationship was not analyzed here, since it
404 requires high temporal resolution model output.

405 An examination of aerosol pH (not presented here) indicated a pH rage from 1 to 2 over EU.
406 This range was recently identified by *Weber et al.* [2016] as a buffering pH zone where
407 partitioning of ammonium nitrate between the gas and aerosol phases is sensitive. Thus, ions
408 which affect pH might play an important role in nitrate formation. Hence, taking into
409 consideration crustal and sea salt ions could affect our thermodynamics and partitioning in
410 regions where these ions are abundant, as *Karydis et al.* [2016] demonstrated. However, these
411 are currently tracked as bulk dust and sea salt aerosols in the model. In addition to tracking Na^+,
412 Cl^-, etc. separately, we would need to consider the different time scales of the thermodynamics
413 associated with aerosol size distribution. In the future, we plan to investigate the influence of
414 pH on the results in more detail.

In this paper we have demonstrated the importance of size resolved sulfate chemistry. However, currently we treat nitrate as bulk, as it is computationally expensive to add 15 nitrate tracers. Perhaps underestimation of nitrate is not only a matter of thermodynamics but microphysics as well, and that properly resolving the size distribution, and considering the chemistry that depends on that would improve our simulations.

Acknowledgements. Climate modeling at GISS is supported by the NASA Modeling, Analysis, and Prediction program. Resources supporting this work were provided by the NASA High-End Computing (HEC) Program through the NASA Center for Climate Simulation (NCCS) at Goddard Space Flight Center. SEB and KT acknowledge funding from NASA's Atmospheric Composition Modeling and Analysis Program (ACMAP), contract number NNX15AE36G. We acknowledge the IMPROVE monitoring program for providing data. EMEP measurement data were extracted from the EBAS database, which is maintained and further developed by the Norwegian Institute for Air Research (NILU). We acknowledge the Toolsets for Airborne Data (TAD) website: https://tad.larc.nasa.gov, as well as the https://sites.google.com/site/amsglobaldatabase/ maintained by the Zhang and Jimenez groups.

References

Aan de Brugh, J. M. J., Henzing, J. S., Schaap, M., Morgan, W. T., van Heerwaarden, C. C., Weijers, E. P., Coe, H. and Krol, M. C.: Modelling the partitioning of ammonium nitrate in the convective boundary layer, Atmos. Chem. Phys., 12(6), 3005–3023, doi:10.5194/acp-12-3005-2012, 2012.

Adams, P. J., Seinfeld, J. H. and Koch, D. M.: Global concentrations of tropospheric sulfate, nitrate, and ammonium aerosol simulated in a general circulation model, J. Geophys. Res., 104, 13791–13823, 1999.

Allan, J. D., Jimenez, J. L., Williams, P. I., Alfarra, M. R., Bower, K. N., Jayne, J. T., Coe, H. and Worsnop, D. R.: Quantitative sampling using an Aerodyne aerosol mass spectrometer: 1. Techniques of data interpretation and error analysis, J. Geophys. Res., 108, doi:10.1029/2003JD001608, 2003.

Anderson, D. C., Loughner, C. P., Diskin, G., Weinheimer, A., Canty, T. P., Salawitch, R. J., Worden, H. M., Fried, A., Mikoviny, T., Wisthaler, A. and Dickerson, R. R.: Measured and modeled CO and NOy in DISCOVER-AQ: An evaluation of emissions and chemistry over the eastern US, Atmos. Environ., 96, 78–87, doi:10.1016/j.atmosenv.2014.07.004, 2014.

447 Bauer, S. E. and Koch, D.: Impact of heterogeneous sulfate formation at mineral dust surfaces
448 on aerosol loads and radiative forcing in the Goddard Institute for Space Studies general
449 circulation model, J. Geophys. Res. D Atmos., 110, 91–105, doi:10.1029/2005JD005870, 2005.

450 Bauer, S. E. and Menon, S.: Aerosol direct , indirect , semidirect , and surface albedo effects
451 from sector contributions based on the IPCC AR5 emissions for preindustrial and present-day
452 conditions, , 117, 1–15, doi:10.1029/2011JD016816, 2012.

453 Bauer, S. E., Balkanaki, Y., Schulz, M. and Hauglustaine, D. A.: Global modeling of
454 heterogeneous chemistry on mineral aerosol surfaces: Influence on tropospheric ozone
455 chemistry and comparison to observations, J. Geophys. Res., 109, 1–17,
456 doi:10.1029/2003JD003868, 2004.

457 Bauer, S. E., Koch, D., Unger, N., Metzger, S. M., Shindell, D. T. and Streets, D. G.: Nitrate
458 aerosols today and in 2030: a global simulation including aerosols and tropospheric ozone,
459 Atmos. Chem. Phys., 7, 5043–5059, doi:10.5194/acp-7-5043-2007, 2007.

460 Bauer, S. E., Wright, D., Koch, D., Lewis, E. R., McGraw, R., Chang, L.-S., Schwartz, S. E. and
461 Ruedy, R.: MATRIX (Multiconfiguration Aerosol TRacker of mIXing state): an aerosol
462 microphysical module for global atmospheric models, Atmos. Chem. Phys., 8, 6003–6035,
463 doi:10.5194/acpd-8-9931-2008, 2008.

464 Benduhn, F., Mann, G. W., Pringle, K. J., Topping, D. O., Mcfiggans, G. and Carslaw, K. S.: Size-
465 resolved simulations of the aerosol inorganic composition with the new hybrid dissolution
466 solver HyDiS-1 . 0 – Description , evaluation and first global modelling results, , (February), 1–
467 54, doi:10.5194/gmd-2015-264, 2016.

468 Conant, W. C., Vanreken, T. M., Rissman, T. A., Varutbangkul, V., Jonsson, H. H., Nenes, A.,
469 Jimenez, J. L., Delia, A. E., Bahreini, R., Roberts, G. C. and Flagan, R. C.: Aerosol--cloud drop
470 concentration closure in warm cumulus, , 109, 1–12, doi:10.1029/2003JD004324, 2004.

471 van Damme, M., Erisman, J. W., Clarisse, L., Dammers, E., Whitburn, S., Clerbaux, C., Dolman, A.
472 J. and Coheur, P.: Worldwide spatiotemporal atmospheric ammonia (NH3) columns variability
473 revealed by satellite, , 1–9, doi:10.1002/2015GL065496.We, 2015.

474 DeCarlo, P. F., Dunlea, E. J., Kimmel, J. R., Aiken, A. C., Sueper, D., Crounse, J., Wennberg, P. O.,
475 Emmons, L., Shinozuka, Y., Clarke, A., Zhou, J., Tomlinson, J., Collins, D. R., Knapp, D.,
476 Weinheimer, A. J., Montzka, D. D., Campos, T. and Jimenez, J. L.: Fast airborne aerosol size and
477 chemistry measurements above Mexico City and Central Mexico during the MILAGRO
478 campaign, Atmos. Chem. Phys., 8(14), 4027–4048, doi:10.5194/acp-8-4027-2008, 2008.

479 Dentener, F., Drevet, J., Lamarque, J. F., Bey, I., Eickhout, B., Fiore, a. M., Hauglustaine, D.,

480 Horowitz, L. W., Krol, M., Kulshrestha, U. C., Lawrence, M., Galy-Lacaux, C., Rast, S., Shindell, D.,
481 Stevenson, D., Van Noije, T., Atherton, C., Bell, N., Bergman, D., Butler, T., Cofala, J., Collins, B.,
482 Doherty, R., Ellingsen, K., Galloway, J., Gauss, M., Montanaro, V., Müller, J. F., Pitari, G.,
483 Rodriguez, J., Sanderson, M., Solmon, F., Strahan, S., Schultz, M., Sudo, K., Szopa, S. and Wild,
484 O.: Nitrogen and sulfur deposition on regional and global scales: A multimodel evaluation,
485 Global Biogeochem. Cycles, 20(4), n/a–n/a, doi:10.1029/2005GB002672, 2006.

486 EMEP: EMEP Manual for Sampling and Analysis, EMEP, available at: http://www.nilu.no/
487 projects/ccc/manual/index.html (last access: 30 October 2015), 2014. 29714, 29723

488 Emmons, L. K., Hauglustaine, D. a., Müller, J.-F., Carroll, M. A., Brasseur, G. P., Brunner, D.,
489 Staehelin, J., Thouret, V. and Marenco, A.: Data composites of airborne observations of
490 tropospheric ozone and its precursors, J. Geophys. Res., 105, 20497,
491 doi:10.1029/2000JD900232, 2000.

492 Fehsenfeld, F. C., Ancellet, G., Bates, T. S., Goldstein, a. H., Hardesty, R. M., Honrath, R., Law, K.
493 S., Lewis, a. C., Leaitch, R., McKeen, S., Meagher, J., Parrish, D. D., Pszenny, a. a P., Russell, P.
494 B., Schlager, H., Seinfeld, J., Talbot, R. and Zbinden, R.: International Consortium for
495 Atmospheric Research on Transport and Transformation (ICARTT): North America to Europe -
496 Overview of the 2004 summer field study, J. Geophys. Res. Atmos., 111,
497 doi:10.1029/2006JD007829, 2006.

498 Fisher, J. a., Jacob, D. J., Purdy, M. T., Kopacz, M., Le Sager, P., Carouge, C., Holmes, C. D.,
499 Yantosca, R. M., Batchelor, R. L., Strong, K., Diskin, G. S., Fuelberg, H. E., Holloway, J. S., Hyer, E.
500 J., McMillan, W. W., Warner, J., Streets, D. G., Zhang, Q., Wang, Y. and Wu, S.: Source
501 attribution and interannual variability of Arctic pollution in spring constrained by aircraft
502 (ARCTAS, ARCPAC) and satellite (AIRS) observations of carbon monoxide, Atmos. Chem. Phys.,
503 10, 977–996, doi:10.5194/acpd-9-19035-2009, 2010.

504 Fountoukis, C. and Nenes, a: ISORROPIA II: a computationally efficient thermodynamic
505 equilibrium model for K+–Ca2+–Mg2+–NH4+–Na+–SO42−–NO3−–Cl−–H2O aerosols, Atmos.
506 Chem. Phys., 7, 4639–4659, doi:10.5194/acp-7-4639-2007, 2007.

507 Hand, J. L., Copeland, S. a., Day, D. E., Dillner, A. M., Indresand, H., Malm, W. C., McDade, C. E.,
508 Moore, C. T., Pitchford, M. L., Schichtel, B. a. and Watson, J. G.: Spatial and Seasonal Patterns
509 and Temporal Variability of Haze and its Constituents in the United States Report V., 2011.

510 Hand, J. L., Schichtel, B. A., Pitchford, M., Malm, W. C. and Frank, N. H.: Seasonal composition of
511 remote and urban fine particulate matter in the United States, J. Geophys. Res., 117(D5),
512 D05209, doi:10.1029/2011JD017122, 2012.

513 Hauglustaine, D. a., Balkanski, Y. and Schulz, M.: A global model simulation of present and

514 future nitrate aerosols and their direct radiative forcing of climate, Atmos. Chem. Phys., 14(20),
515 11031–11063, doi:10.5194/acp-14-11031-2014, 2014.

516 Haywood, J. and Boucher, O.: Estimates of the Direct and Indirect Radiative Forcing Due to
517 Tropospheric Aerosols: A Review, Rev. Geophys., 38(4), 513–543, 2000.

518 Heald, C. L., Jacob, D. J., Park, R. J., Russell, L. M., Huebert, B. J., Seinfeld, J. H., Liao, H. and
519 Weber, R. J.: A large organic aerosol source in the free troposphere missing from current
520 models, Geophys. Res. Lett., 32(18), 1–4, doi:10.1029/2005GL023831, 2005.

521 Heald, C. L., Coe, H., Jimenez, J. L., Weber, R. J., Bahreini, R., Middlebrook, a. M., Russell, L. M.,
522 Jolleys, M., Fu, T.-M., Allan, J. D., Bower, K. N., Capes, G., Crosier, J., Morgan, W. T., Robinson,
523 N. H., Williams, P. I., Cubison, M. J., DeCarlo, P. F. and Dunlea, E. J.: Exploring the vertical profile
524 of atmospheric organic aerosol: comparing 17 aircraft field campaigns with a global model,
525 Atmos. Chem. Phys., 11(24), 12673–12696, doi:10.5194/acp-11-12673-2011, 2011.

526 Hodas, N., Sullivan, A. P., Skog, K., Keutsch, F. N., Collett, J. L., Decesari, S., Facchini, M. C.,
527 Carlton, A. G., Laaksonen, A. and Turpin, B. J.: Aerosol liquid water driven by anthropogenic
528 nitrate: implications for lifetimes of water-soluble organic gases and potential for secondary
529 organic aerosol formation., Environ. Sci. Technol., 48(19), 11127–36, doi:10.1021/es5025096,
530 2014.

531 Huebert, B. J.: An overview of ACE-Asia: Strategies for quantifying the relationships between
532 Asian aerosols and their climatic impacts, J. Geophys. Res., 108(D23), 8633,
533 doi:10.1029/2003JD003550, 2003.

534 Ichoku, C. and Ellison, L.: Global top-down smoke-aerosol emissions estimation using satellite
535 fire radiative power measurements, Atmos. Chem. Phys., 14, 6643–6667, doi:10.5194/acp-14-
536 6643-2014, 2014.

537 Jacob, D. J., Crawford, J. H., Maring, H., Clarke, a. D., Dibb, J. E., Emmons, L. K., Ferrare, R. a.,
538 Hostetler, C. a., Russell, P. B., Singh, H. B., Thompson, a. M., Shaw, G. E., McCauley, E.,
539 Pederson, J. R. and Fisher, J. a.: The arctic research of the composition of the troposphere from
540 aircraft and satellites (ARCTAS) mission: Design, execution, and first results, Atmos. Chem.
541 Phys., 10, 5191–5212, doi:10.5194/acp-10-5191-2010, 2010.

542 Jimenez, J. L., Jayne, J. T., Shi, Q., Kolb, C. E., Worsnop, D. R., Yourshaw, I., Seinfeld, J. H., Flagan,
543 R. C., Zhang, X., Smith, K. A., Morris, J. W. and Davidovits, P.: Ambient aerosol sampling using
544 the Aerodyne Aerosol Mass Spectrometer, J. Geophys. Res., 108(D7), 8425,
545 doi:10.1029/2001jd001213, 2003.

546 Kalnay, E., Kanamitsu, M., Kistler, R., Collins, W., Deaven, D., Gandin, L., Iredell, M., Saha, S.,

White, G., Woollen, J., Zhu, Y., Chelliah, M., Ebisuzaki, W., Higgins, W., Janowiak, J., Mo, K. C., Ropelewski, C., Wang, J., Leetmaa, A., Reynolds, R., Jenne, R. and Joseph, D.: The NCEP/NCAR 40-Year Reanalysis Project, Bull. Am. Meteorol. Soc., 77(2), 437–471, 1996.

Karydis, V. a., Tsimpidi, a. P., Pozzer, A., Astitha, M. and Lelieveld, J.: Effects of mineral dust on global atmospheric nitrate concentrations, Atmos. Chem. Phys., 16, 1491–1509, doi:10.5194/acpd-15-11525-2015, 2016.

Koch, D., D. Jacob, I. Tegen, D. Rind, and M. Chin, 1999: Tropospheric sulfur simulation and sulfate direct radiative forcing in the Goddard Institute for Space Studies general circulation model. *J. Geophys. Res.*, **104**, 23799-23822, doi:10.1029/1999JD900248.

Koch, D., Schmidt, G. a. and Field, C. V.: Sulfur, sea salt, and radionuclide aerosols in GISS ModelE, J. Geophys. Res. Atmos., 111(December 2005), doi:10.1029/2004JD005550, 2006.

Konovalov, I. B., Beekmann, M., Burrows, J. P. and Richter, a.: Satellite measurement based estimates of decadal changes in European nitrogen oxides emissions, Atmos. Chem. Phys. Discuss., 8(1), 2013–2059, doi:10.5194/acpd-8-2013-2008, 2008.

Lamarque, J.-F., Bond, T. C., Eyring, V., Granier, C., Heil, A., Klimont, Z., Lee, D., Liousse, C., Mieville, A., Owen, B., Schultz, M. G., Shindell, D., Smith, S. J., Stehfest, E., Van Aardenne, J., Cooper, O. R., Kainuma, M., Mahowald, N., McConnell, J. R., Naik, V., Riahi, K. and van Vuuren, D. P.: Historical (1850–2000) gridded anthropogenic and biomass burning emissions of reactive gases and aerosols: methodology and application, Atmos. Chem. Phys., 10, 7017–7039, doi:10.5194/acp-10-7017-2010, 2010.

Leaitch, W. R., Macdonald, a. M., Anlauf, K. G., Liu, P. S. K., Toom-Sauntry, D., Li, S.-M., Liggio, J., Hayden, K., Wasey, M. a., Russell, L. M., Takahama, S., Liu, S., van Donkelaar, A., Duck, T., Martin, R. V., Zhang, Q., Sun, Y., McKendry, I., Shantz, N. C. and Cubison, M.: Evidence for Asian dust effects from aerosol plume measurements during INTEX-B 2006 near Whistler, BC, Atmos. Chem. Phys. Discuss., 8, 18531–18589, doi:10.5194/acpd-8-18531-2008, 2009.

Lohmann, U. and Feichter, J.: Global indirect aerosol effects : a review, Atmos. Chem. Phys., 5, 715–737, 2005.

Malm, W. C., Sisler, J. F., Huffman, D., Eldred, R. A. and Cahill, T. A.: SPATIAL AND SEASONAL TRENDS IN PARTICLE CONCENTRATION AND OPTICAL EXTINCTION IN THE UNITED-STATES, J. Geophys. Res., 99, 1347–1370, 1994.

Malm, W. C., Schichtel, B. A., Pitchford, M. L., Ashbaugh, L. L. and Eldred, R. A.: Spatial and monthly trends in speciated fine particle concentration in the United States, J. Geophys. Res., 109, doi:10.1029/2003JD003739, 2004.

Metzger, S., Dentener, F., Krol, M., Jeuken, A. and Lelieveld, J.: Gas/aerosol partitioning 2. Global modeling results, J. Geophys. Res. D Atmos., 107(August), 1–23, 2002a.

Metzger, S., Dentener, F., Pandis, S. and Lelieveld, J.: Gas/aerosol partitioning: 1. A computationally efficient model, J. Geophys. Res. Atmos., 107(August), doi:10.1029/2001JD001102, 2002b.

Miller, R. L., Cakmur, R. V., Perlwitz, J., Geogdzhayev, I. V., Ginoux, P., Koch, D., Kohfeld, K. E., Prigent, C., Ruedy, R., Schmidt, G. a. and Tegen, I.: Mineral dust aerosols in the NASA Goddard Institute for Space Sciences ModelE atmospheric general circulation model, J. Geophys. Res. Atmos., 111, 1–19, doi:10.1029/2005JD005796, 2006.

Morgan, W. T., Allan, J. D., Bower, K. N., Esselborn, M., Harris, B., Henzing, J. S., Highwood, E. J., Kiendler-Scharr, a., McMeeking, G. R., Mensah, a. a., Northway, M. J., Osborne, S., Williams, P. I., Krejci, R. and Coe, H.: Enhancement of the aerosol direct radiative effect by semi-volatile aerosol components: airborne measurements in North-Western Europe, Atmos. Chem. Phys., 10(17), 8151–8171, doi:10.5194/acp-10-8151-2010, 2010.

Park, R. J.: Natural and transboundary pollution influences on sulfate-nitrate-ammonium aerosols in the United States: Implications for policy, J. Geophys. Res., 109(D15), D15204, doi:10.1029/2003JD004473, 2004.

Parrish, D. D., Allen, D. T., Bates, T. S., Estes, M., Fehsenfeld, F. C., Feingold, G., Ferrare, R., Hardesty, R. M., Meagher, J. F., Nielsen-Gammon, J. W., Pierce, R. B., Ryerson, T. B., Seinfeld, J. H. and Williams, E. J.: Overview of the second texas air quality study (TexAQS II) and the Gulf of Mexico atmospheric composition and climate study (GoMACCS), J. Geophys. Res. Atmos., 114, 1–28, doi:10.1029/2009JD011842, 2009.

Paulot, F., Jacob, D. J., Pinder, R. W., Bash, J. O., Travis, K. and Henze, D. K.: Ammonia emissions in the United States, European Union, and China derived by high-resolution inversion of ammonium wet deposition data: Interpretation with a new agricultural emissions inventory (MASAGE-NH3), J. Geophys. Res. Atmos., 119(7), 4343–4364, doi:10.1002/2013JD021130, 2014.

Paulot, F., Ginoux, P., Cooke, W. F., Donner, L. J., Fan, S., Lin, M., Mao, J., Naik, V. and Horowitz, L. W.: Sensitivity of nitrate aerosols to ammonia emissions and to nitrate chemistry: implications for present and future nitrate optical depth, Atmos. Chem. Phys., 15(18), 25739–25788, doi:10.5194/acpd-15-25739-2015, 2016.

Potukuchi, S. and Wexler, A. S.: Identifying solid-aqueous-phase transitions in atmospheric aerosols. II. Acidic solutions, Atmos. Environ., 29(22), 3357–3364, doi:10.1016/1352-2310(95)00212-H, 1995a.

613 Potukuchi, S. and Wexler, S. A.: Identifying solid-aqueous-phase transitions in atmospheric
614 aerosols. I. Neutral-acidity solutions, Atmos. Environ., 29(14), 1995b.

615 Pusede, S. E., Duffey, K. C., Shusterman, a. a., Saleh, A., Laughner, J. L., Wooldridge, P. J., Zhang,
616 Q., Parworth, C. L., Kim, H., Capps, S. L., Valin, L. C., Cappa, C. D., Fried, A., Walega, J., Nowak, J.
617 B., Hoff, R. M., Berkoff, T. a., Beyersdorf, a. J., Olson, J., Crawford, J. H. and Cohen, R. C.: On the
618 effectiveness of nitrogen oxide reductions as a control over ammonium nitrate aerosol, Atmos.
619 Chem. Phys., 15(19), 27087–27136, doi:10.5194/acpd-15-27087-2015, 2016.

620 Ravishankara, A. R.: Heterogeneous and Multiphase Chemistry in the Troposphere, Science (80-
621 .)., 276(5315), 1058–1065, doi:10.1126/science.276.5315.1058, 1997.

622 Rayner, N. A., Parker, D. E., Horton, E. B., Folland, C. K., Alexander, L. V., Rowell, D. P., Kent, E. C.
623 and Kaplan, A.: Global analyses of sea surface temperature, sea ice, and night marine air
624 temperature since the late nineteenth century, J. Geophys. Res., 108(D14), 4407,
625 doi:10.1029/2002JD002670, 2003.

626 Ryerson, T. B., Andrews, a. E., Angevine, W. M., Bates, T. S., Brock, C. a., Cairns, B., Cohen, R. C.,
627 Cooper, O. R., De Gouw, J. a., Fehsenfeld, F. C., Ferrare, R. a., Fischer, M. L., Flagan, R. C.,
628 Goldstein, a. H., Hair, J. W., Hardesty, R. M., Hostetler, C. a., Jimenez, J. L., Langford, a. O.,
629 McCauley, E., McKeen, S. a., Molina, L. T., Nenes, a., Oltmans, S. J., Parrish, D. D., Pederson, J.
630 R., Pierce, R. B., Prather, K., Quinn, P. K., Seinfeld, J. H., Senff, C. J., Sorooshian, a., Stutz, J.,
631 Surratt, J. D., Trainer, M., Volkamer, R., Williams, E. J. and Wofsy, S. C.: The 2010 California
632 Research at the Nexus of Air Quality and Climate Change (CalNex) field study, J. Geophys. Res.
633 Atmos., 118, 5830–5866, doi:10.1002/jgrd.50331, 2013.

634 Schaap, M., van Loon, M., ten Brink, H. M., Dentener, F. J. and Builtjes, P. J. H.: Secondary
635 inorganic aerosol simulations for Europe with special attention to nitrate, Atmos. Chem. Phys.,
636 4(3), 857–874, doi:10.5194/acp-4-857-2004, 2004.

637 Schmidt, G. a, Kelley, M., Nazarenko, L., Ruedy, R., Russell, G. L., Aleinov, I., Bauer, M., Bauer, S.
638 E., Bhat, M. K., Bleck, R., Canuto, V., Chen, Y., Cheng, Y., Clune, T. L., Genio, A. Del, Fainchtein, R.
639 De, Faluvegi, G., Hansen, J. E., Healy, R. J., Kiang, N. Y., Koch, D., Lacis, A. a, Legrande, A. N.,
640 Lerner, J., Lo, K. K., Matthews, E. E., Menon, S., Miller, R. L., Oinas, V., Oloso, A. O., Perlwitz, J.
641 P., Puma, M. J., Putman, W. M., Rind, D., Romanou, A., Sato, M., Shindell, D. T., Sun, S., Syed, R.
642 A., Tausnev, N., Tsigaridis, K., Unger, N., Voulgarakis, A., Yao, M.-S. and Zhang, J.: Configuration
643 and assessment of the GISS ModelE2 contributions to the CMIP5 archive, J. Adv. Model. Earth
644 Syst., 6, 141–184, doi:10.1002/2013MS000265.Received, 2014.

645 Shindell, D. T., Garenfell, L. J., Rind, D., Grewel, V. and Price, C.: Chemistry-climate interactions
646 in the Goddard Institute for Space Studies general circulation model 1. Tropospheric chemistry

model description and evaluation, J. Geophys. Res., 106(D8), 8047–8075, 2001.

Shindell, D. T., Faluvegi, G. and Bell, N.: Preindustrial-to-present-day radiative forcing by tropospheric ozone from improved simulations with the GISS chemistry-climate GCM, Atmos. Chem. Phys., 3, 3939–3989, doi:10.5194/acpd-3-3939-2003, 2003.

Shindell, D. T., Faluvegi, G., Aguilar, E., Schmidt, G. A., Koch, D. M., Bauer, S. E. and Miller, R. L.: Simulations of preindustrail, present-day, and 2100 conditions in the NASA GISS composition and climate model G-PUCCINI, Atmos. Chem. Phys., 6, 4427–4459, 2006.

Shindell, D. T., Lamarque, J. F., Schulz, M., Flanner, M., Jiao, C., Chin, M., Young, P. J., Lee, Y. H., Rotstayn, L., Mahowald, N., Milly, G., Faluvegi, G., Balkanski, Y., Collins, W. J., Conley, a. J., Dalsoren, S., Easter, R., Ghan, S., Horowitz, L., Liu, X., Myhre, G., Nagashima, T., Naik, V., Rumbold, S. T., Skeie, R., Sudo, K., Szopa, S., Takemura, T., Voulgarakis, a., Yoon, J. H. and Lo, F.: Radiative forcing in the ACCMIP historical and future climate simulations, Atmos. Chem. Phys., 13(6), 2939–2974, doi:10.5194/acp-13-2939-2013, 2013.

Singh, H. B., Brune, W. H., Crawford, J. H., Jacob, D. J. and Russell, P. B.: Overview of the summer 2004 Intercontinental Chemical Transport Experiment-North America (INTEX-A), J. Geophys. Res. Atmos., 111(December), doi:10.1029/2006JD007905, 2006.

Stocker, T. F., D. Qin, G.-K. Plattner, M. Tignor, S.K. Allen, J. Boschung, A. Nauels, Y. Xia, V. Bex and P.M. Midgley (eds.): IPCC, 2013: Summary for Policymakers. In: Climate Change 2013: The Physical Science Basis. Contribution of Working Group I to the Fifth Assessment Report of the Intergovernmental Panel on Climate Change, Cambridge University Press, Cambridge, United Kingdom and New York, NY, USA., 2013.

Tagaris, E., Manomaiphiboon, K., Liao, K. J., Leung, L. R., Woo, J. H., He, S., Amar, P. and Russell, A. G.: Impacts of global climate change and emissions on regional ozone and fine particulate matter concentrations over the United States, J. Geophys. Res. Atmos., 112, doi:10.1029/2006JD008262, 2007.

Tørseth, K., Aas, W., Breivik, K., Fjeraa, A. M., Fiebig, M., Hjellbrekke, A. G., Lund Myhre, C., Solberg, S. and Yttri, K. E.: Introduction to the European Monitoring and Evaluation Programme (EMEP) and observed atmospheric composition change during 1972-2009, Atmos. Chem. Phys., 12(12), 5447–5481, doi:10.5194/acp-12-5447-2012, 2012.

Vestreng, V., Myhre, G., Fagerli, H., Reis, S. and Tarrasón, L.: Twenty-five years of continuous sulphur dioxide emission reduction in Europe, Atmos. Chem. Phys., 7(13), 3663–3681, doi:10.5194/acp-7-3663-2007, 2007.

van Vuuren, D. P., Edmonds, J., Kainuma, M., Riahi, K., Thomson, A., Hibbard, K., Hurtt, G. C.,

Kram, T., Krey, V., Lamarque, J. F., Masui, T., Meinshausen, M., Nakicenovic, N., Smith, S. J. and Rose, S. K.: The representative concentration pathways: An overview, Clim. Change, 109, 5–31, doi:10.1007/s10584-011-0148-z, 2011.

Weber, R. J., Orsini, D., Daun, Y., Lee, Y.-N., Klotz, P. J. and Brechtel, F.: A Particle-into-Liquid Collector for Rapid Measurement of Aerosol Bulk Chemical Composition, Aerosol Sci. Technol., 35(February 2015), 718–727, doi:10.1080/02786820152546761, 2001.

Weber, R. J., Guo, H., Russell, A. G. and Nenes, A.: High aerosol acidity despite declining atmospheric sulfate concentrations over the past 15 years, Nat. Geosci., doi:10.1038/NGEO2665, 2016.

van der Werf, G. R., Randerson, J. T., Giglio, L., Collatz, G. J., Mu, M., Kasibhatla, P. S., Morton, D. C., Defries, R. S., Jin, Y. and van Leeuwen, T. T.: Global fire emissions and the contribution of deforestation, savanna, forest, agricultural, and peat fires (1997-2009), Atmos. Chem. Phys., 10, 11707–11735, doi:10.5194/acp-10-11707-2010, 2010.

Xu, L. and Penner, J. E.: Global simulations of nitrate and ammonium aerosols and their radiative effects, Atmos. Chem. Phys., 12(20), 9479–9504, doi:10.5194/acp-12-9479-2012, 2012.

Ziemba, L. D., Thornhill, K. L., Ferrare, R., Barrick, J., Beyersdorf, A. J., Chen, G., Crumeyrolle, S. N., Hair, J., Hostetler, C., Hudgins, C., Obland, M., Rogers, R., Scarino, A. J., Winstead, E. L. and Anderson, B. E.: Airborne observations of aerosol extinction by in situ and remote-sensing techniques: Evaluation of particle hygroscopicity, Geophys. Res. Lett., 40(2), 417–422, doi:10.1029/2012GL054428, 2013.

Table 1. Regional boundaries for data division

Region	Boundaries
Arctic (ARC)	55°-90°N, 60°-170°W
Eastern USA (EUSA)	30°-50°N, 60°-95°W
Western USA (WUSA)	30°-50°N, 114°-130°W
European Union (EU)	35°-70°N, 10°W-30°E

742
743
744
745
746
747
748
749
750 **Table 2.** Airborne measurements used in this study.
751
752

Campaign (Aircraft)	Region (season, year)	Technique and reference	Regime
ACE-Asia (CIPRAS TWIN OTTER)	Japan (spring, 2001)	AMS (Huebert, 2003)	Polluted
CRYSTAL-FACE (CIPRAS TWIN OTTER)	South Florida (summer, 2002)	AMS (Conant et al., 2004)	Polluted
ITOP (BAE-146)	Azores (summer, 2004)	AMS (Fehsenfeld et al., 2006)	Remote
INTEX-A (DC-8, J-31)	Eastern USA (summer, 2004)	CIMS (HNO_3), PILS (SO_4,NH_4,NO_3) (Singh et al., 2006)	Polluted
NEAQS (NOAA-P3)	Eastern USA (summer, 2004)	CIMS (HNO_3), AMS (SO_4, NH_4, NO_3) (Fehsenfeld et al., 2006)	Polluted
INTEX-B (DC-8)	Western USA (spring, 2006)	CIMS (HNO_3), AMS (SO_4,NH_4,NO_3) (Leaitch et al., 2009)	Polluted
MILAGRO (C120)	Mexico (spring, 2006)	AMS (DeCarlo et al., 2008)	Polluted
TexAQS (NOAA-P3)	Texas (fall, 2006)	CIMS (NH3, HNO_3), AMS (SO_4, NH_4, NO_3) (Parrish et al., 2009)	Polluted
EUCAARI (BAE-146)	NW EU (spring, 2008)	AMS (Morgan et al., 2010)	Polluted
ARCPAC (NOAA-P3	Arctic (spring, 2008)	CIMS (HNO_3), AMS (SO_4, NH_4, NO_3) (Fisher et al., 2010)	Fire
ARCTAS (DC-8, P-3)	Arctic (spring/summer 2008)	CIMS (HNO_3), AMS (SO_4, NH_4, NO_3) (Jacob et al., 2010)	Fire
CALNEX (NOAA P-3)	West coast (summer, 2010)	CIMS (HNO_3, NH_3), AMS (SO_4, NH_4, NO_3) (Ryerson et al., 2013)	Polluted
DISCOVER-MD (P-3B,	Maryland (summer, 2011)	TD-LIF (HNO_3) (Anderson et al., 2014), PILS (SO_4, NH_4, NO_3) (Ziemba et al., 2013)	Polluted

UC-12)

753

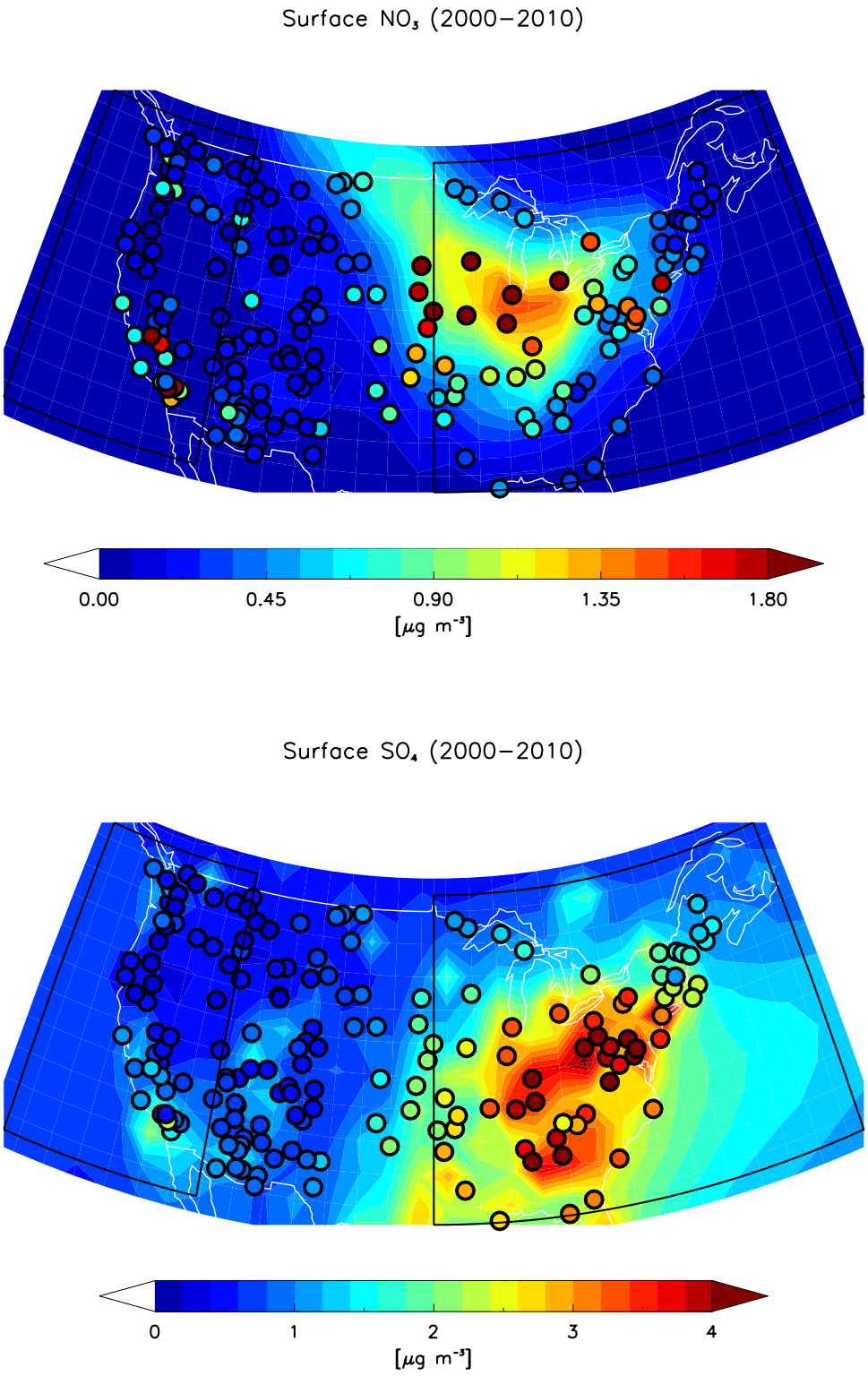

754

755 **Figure 1.** Mean nitrate (upper panel) and sulfate (lower panel) surface concentration (2000-
756 2010) simulated by MATRIX-EQSAM overlaid by measurements from the IMPROVE network.
757 The model data units match the units of the measured data ($\mu g\ m^{-3}$).

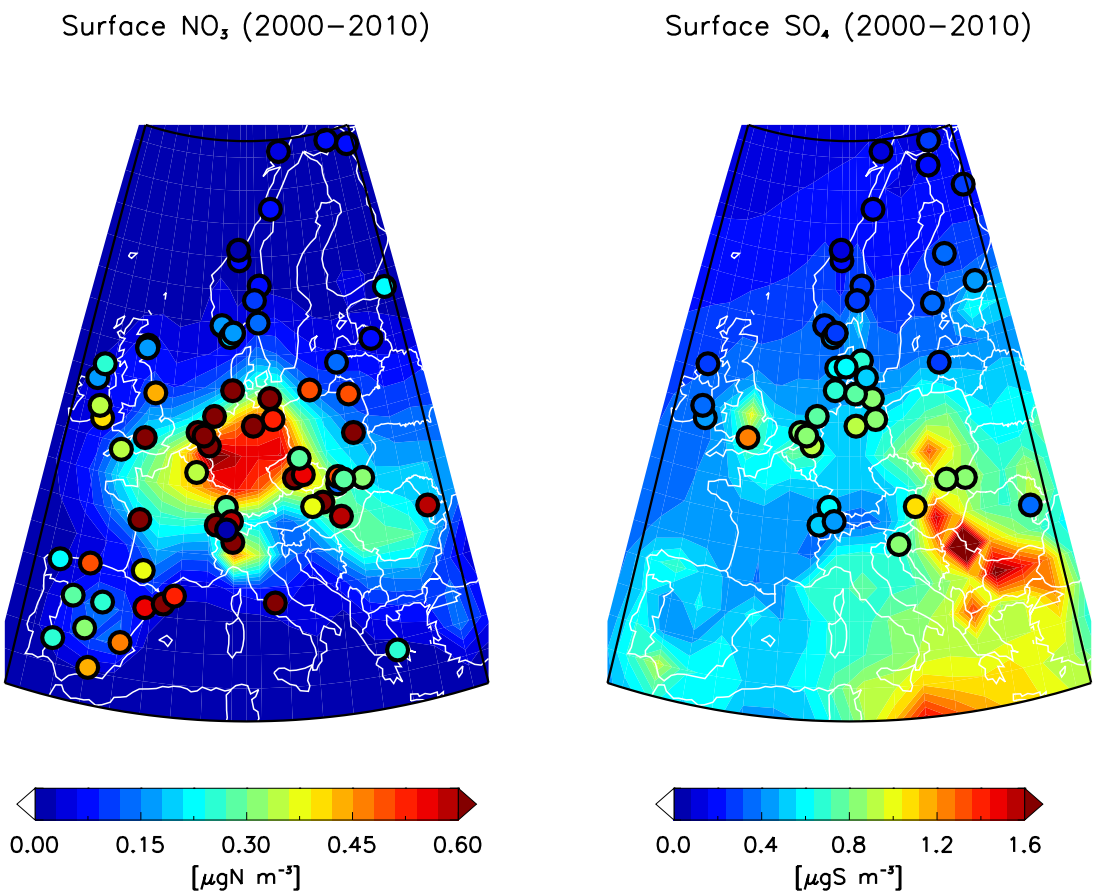

758

759 **Figure 2.** Mean nitrate (right panel) and sulfate (left panel) surface concentration (2000-2010)
760 simulated by MATRIX-EQSAM overlaid by measurements from the EMEP network. The model
761 data units match the units of the measured data (μgX m^{-3} with X being N for nitrate and S for
762 sulfate).

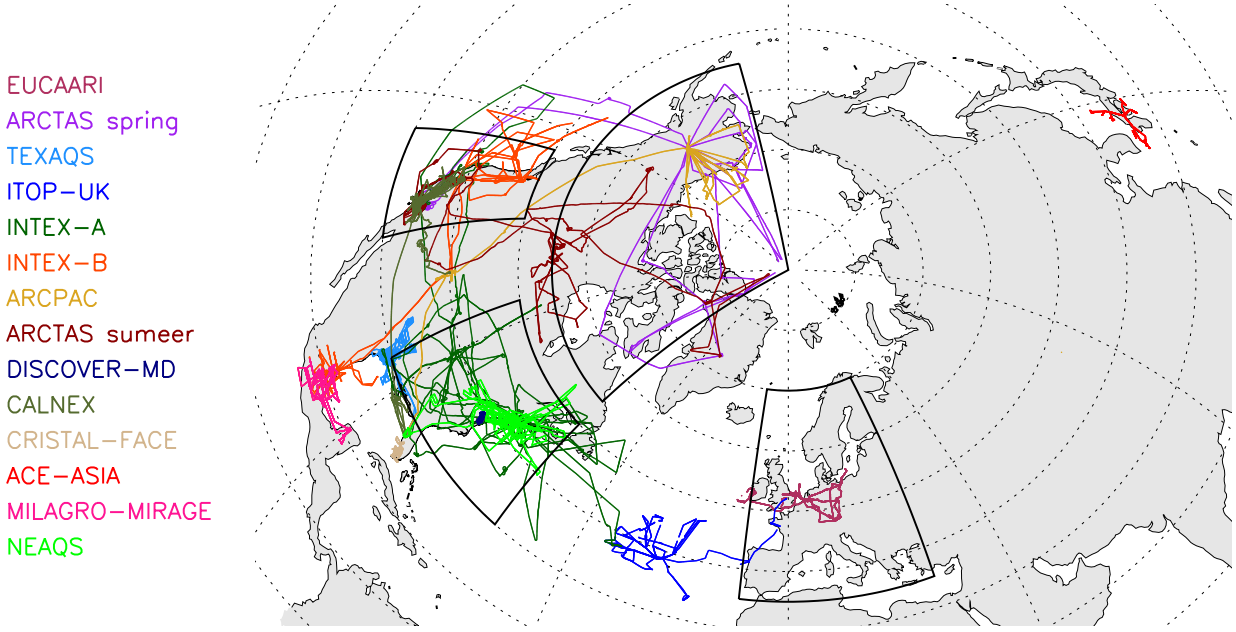

763

764 **Figure 3.** Flight tracks of 14 flight campaigns used in this study (2001-2011).

765

766

767

768

769

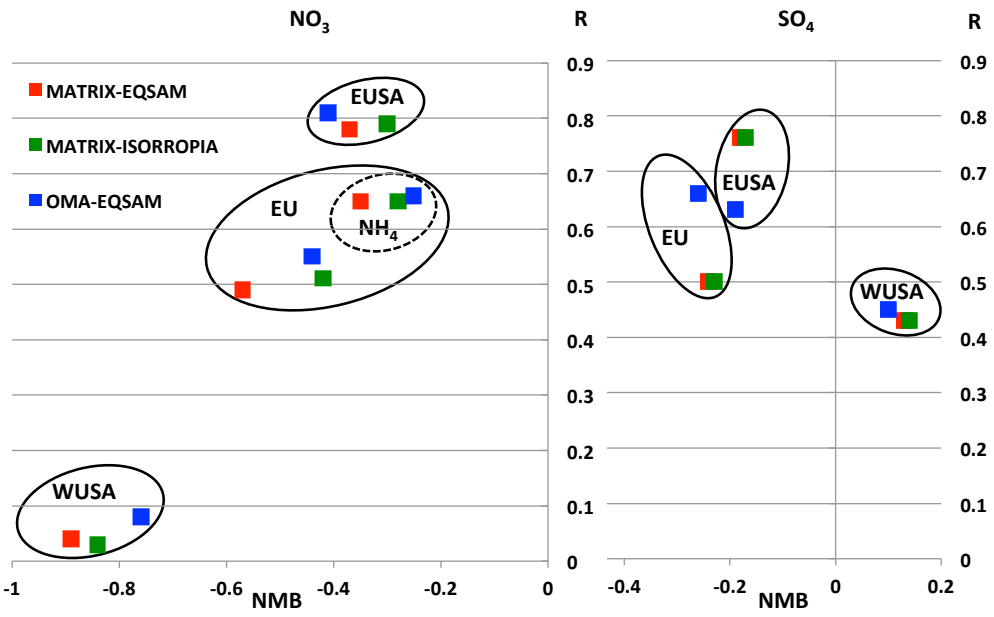

770

771 **Figure 4.** Surface regional statistics (2000-2010). Left panel: nitrate and ammonium (data
772 available only for EU); right panel: sulfate. The correlation coefficient (R) between the
773 simulation and the measurements is in the y-axis, and normalized mean bias (NMB) is in the x-
774 axis. MATRIX-EQSAM is in red, MATRIX-ISORROPIA II is in green and OMA-EQSAM is in blue.

775

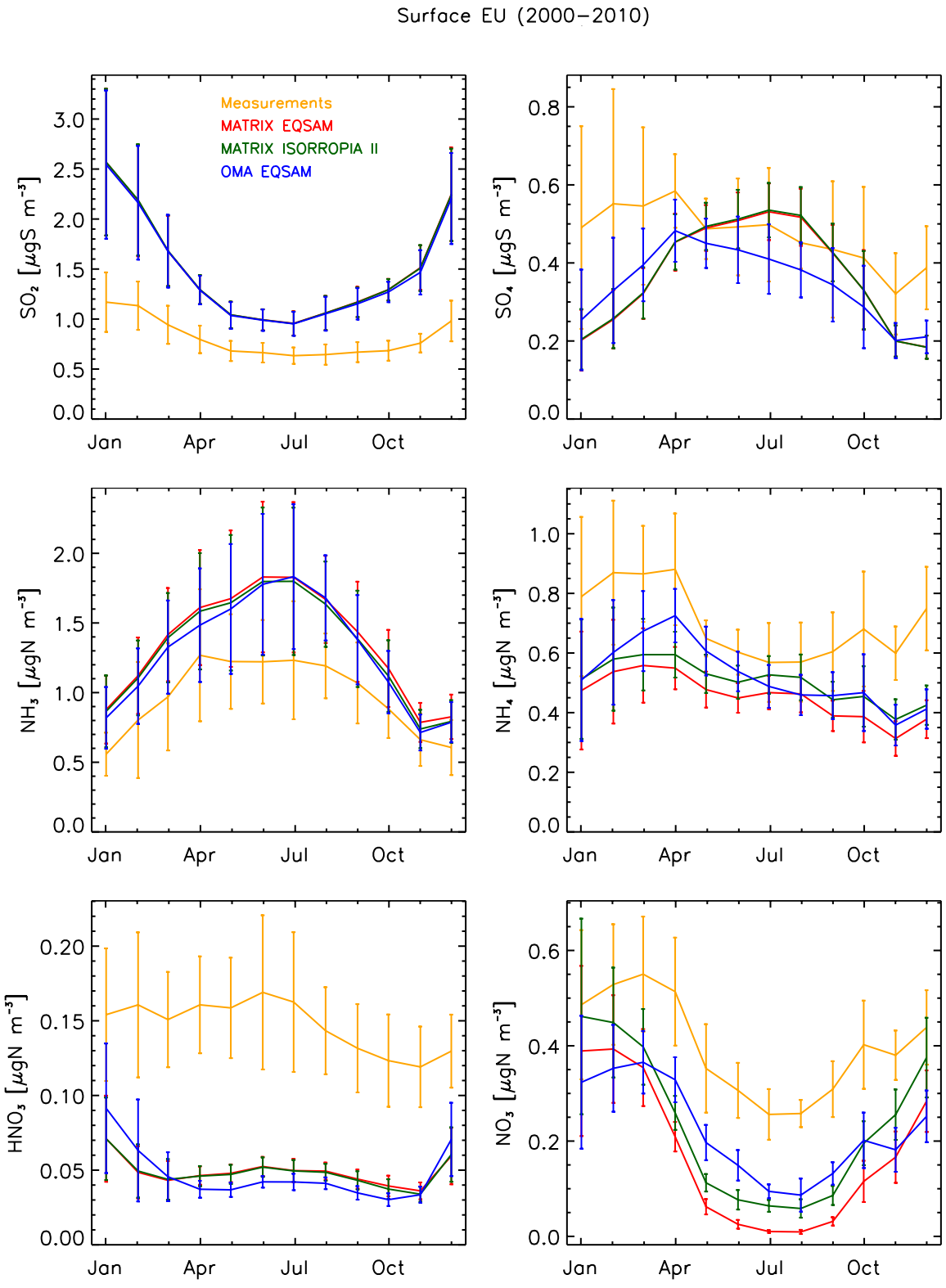

776

777 **Figure 5.** 2000-2010 mean annual cycle over Europe, error bars represent ± one standard
778 deviation. Measurements are in orange, MATRIX-EQSAM is in red, MATRIX-ISORROPIA II is in
779 green and OMA-EQSAM is in blue.

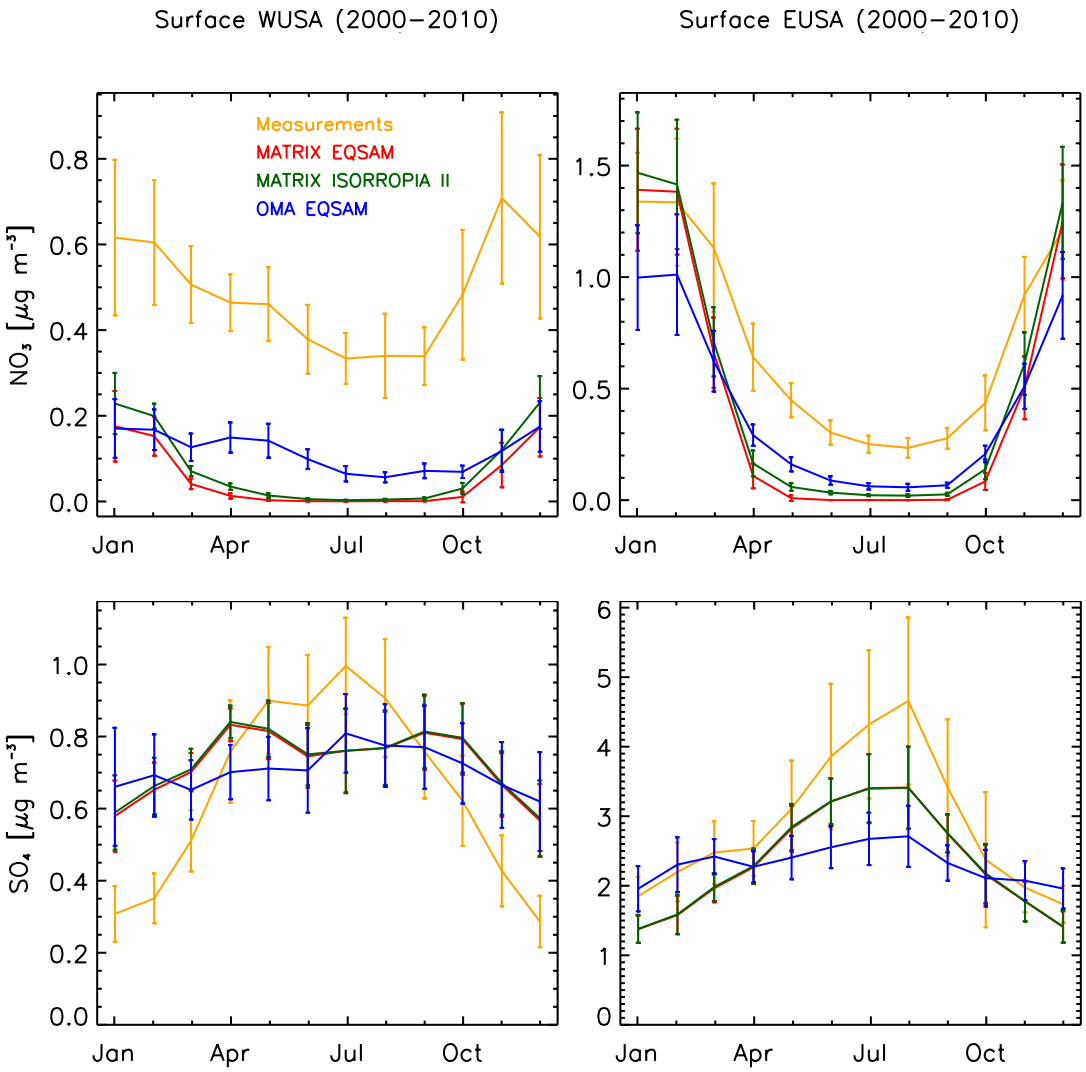

780

781 **Figure 6.** 2000-2010 mean annual cycle over WUSA (left) and EUSA (right), error bars represent
782 ± one standard deviation. Measurements are in orange, MATRIX-EQSAM is in red, MATRIX-
783 ISORROPIA II is in green and OMA-EQSAM is in blue.

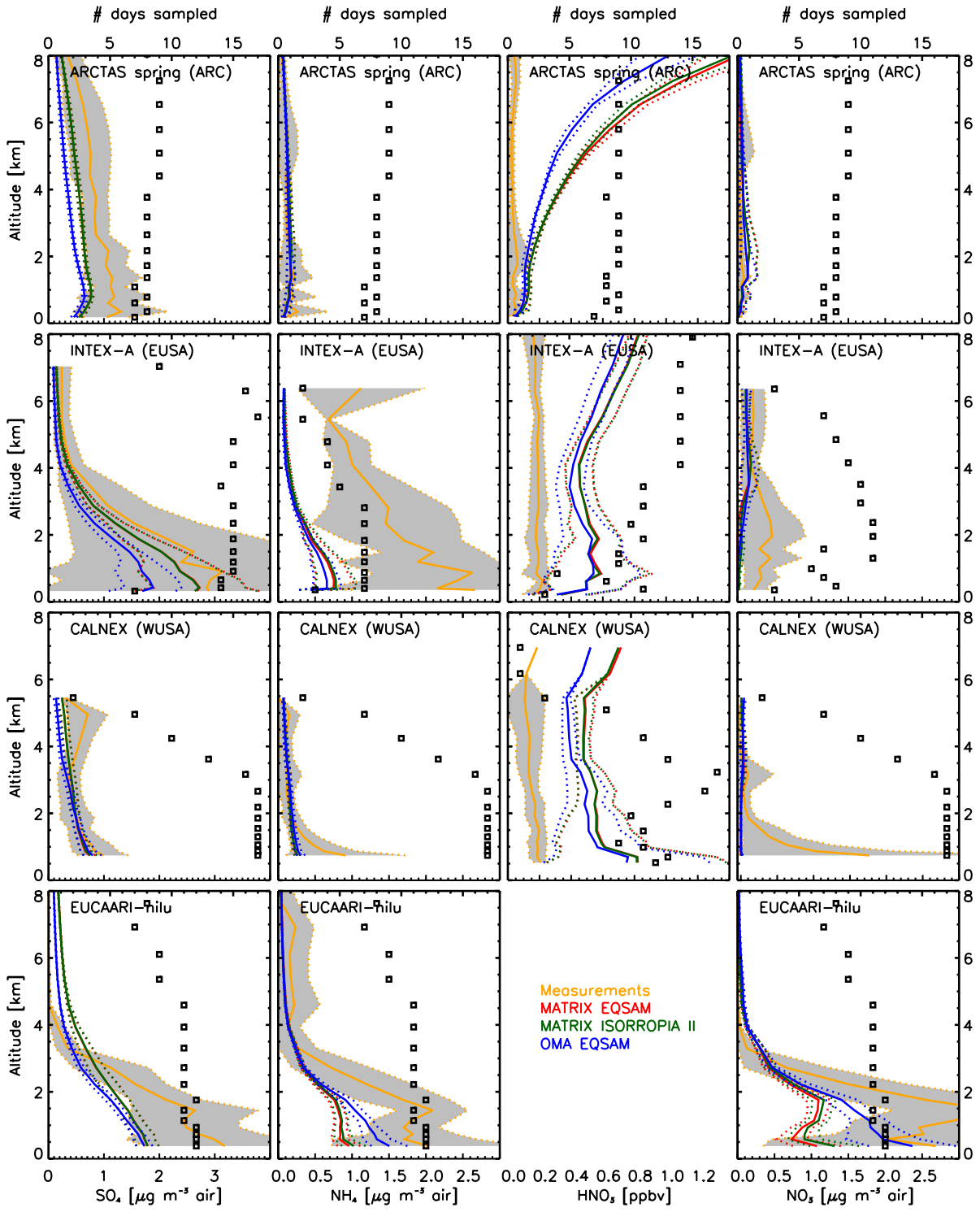

784

785 **Figure 7.** Mean regional concentration profiles from the arctic (first row), eastern USA (second
786 row), western USA (third row) and Europe (fourth row). First column is SO_4, second is NH_4, third
787 is HNO_3 and fourth is NO_3.

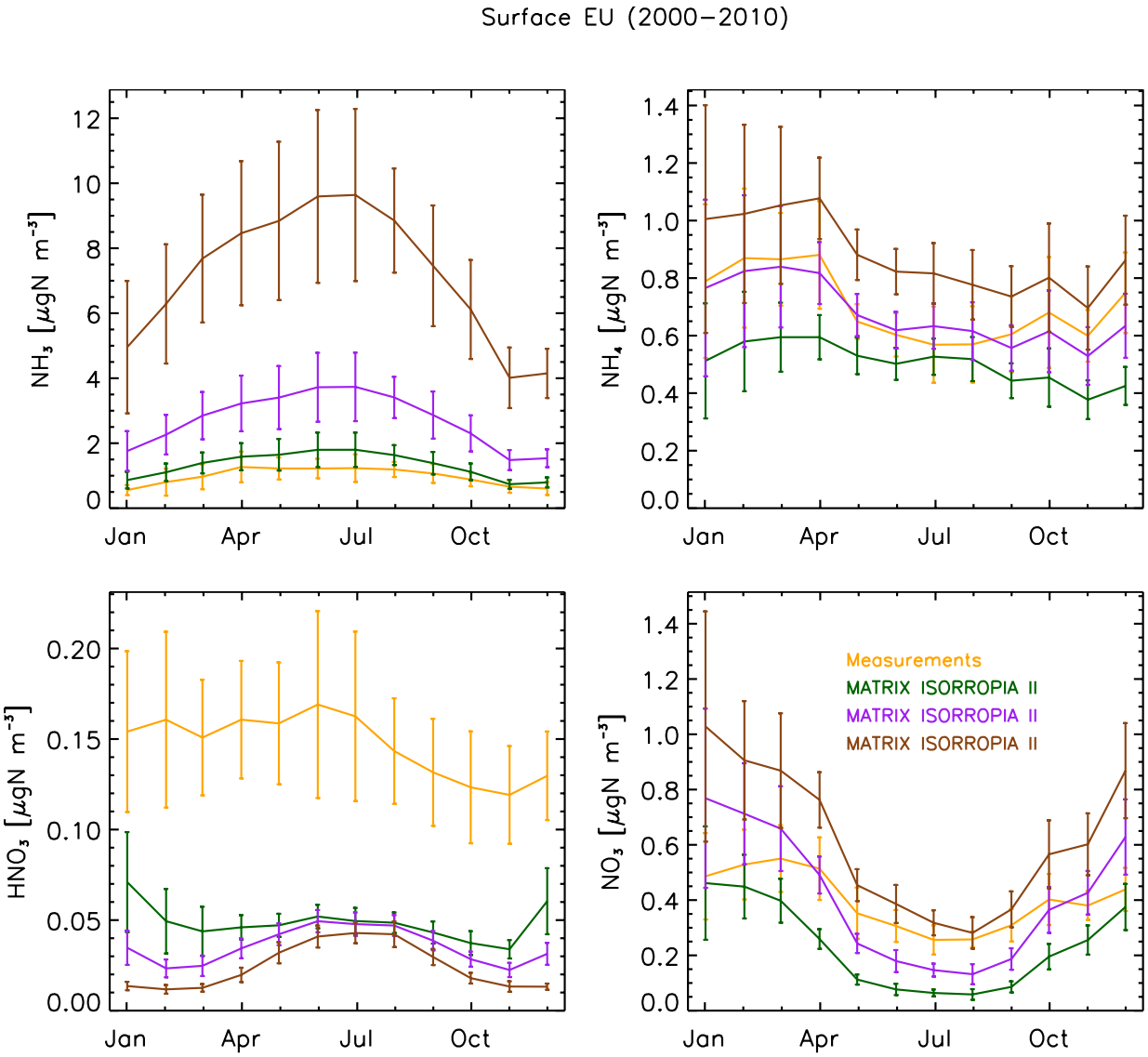

788

789 **Figure 8.** 2000-2010 mean annual cycle over Europe, error bars represent ± one standard
790 deviation. Measurements are in orange, MATRIX-ISORROPIA II: with regular emissions is in
791 green, with double agricultural NH_3 emissions is in purple, and with 5-times agricultural NH_3
792 emissions is in brown.

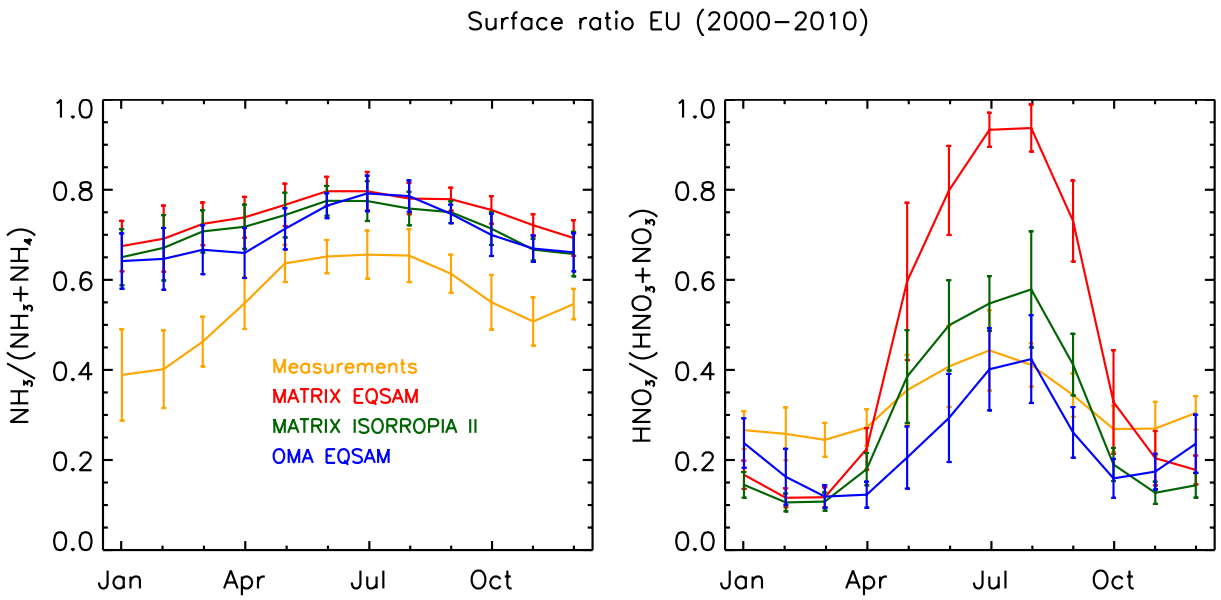

793

794 **Figure 9.** 2000-2010 mean partitioning ratio annul cycle over Europe, error bars represent ±
795 one standard deviation. Measurements are in orange, MATRIX-EQSAM is in red, MATRIX-
796 ISORROPIA II is in green and OMA-EQSAM is in blue.

797

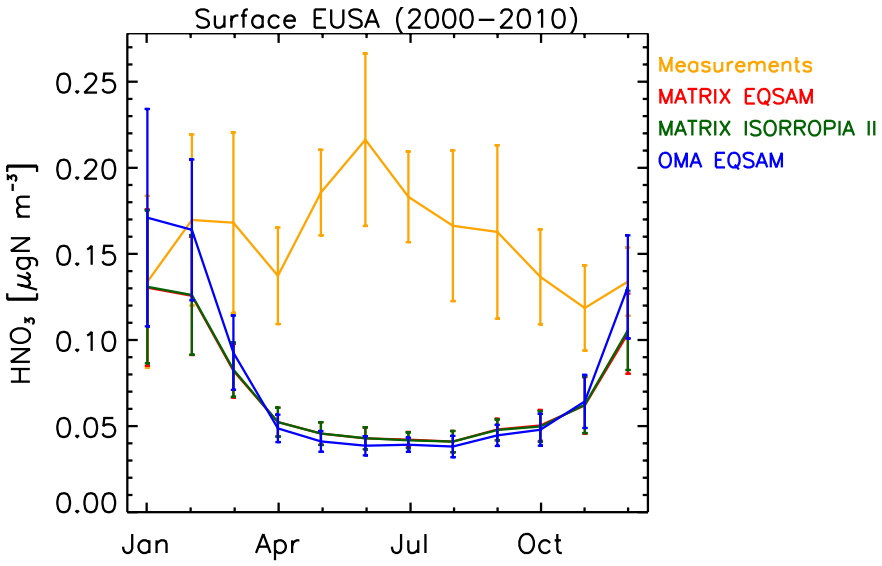

798

799 **Figure A1.** 2000-2010 HNO_3 mean annual cycle over EUSA (right), error bars represent ± one
800 standard deviation. Measurements are in orange, MATRIX-EQSAM is in red, MATRIX-ISORROPIA
801 II is in green and OMA-EQSAM is in blue.

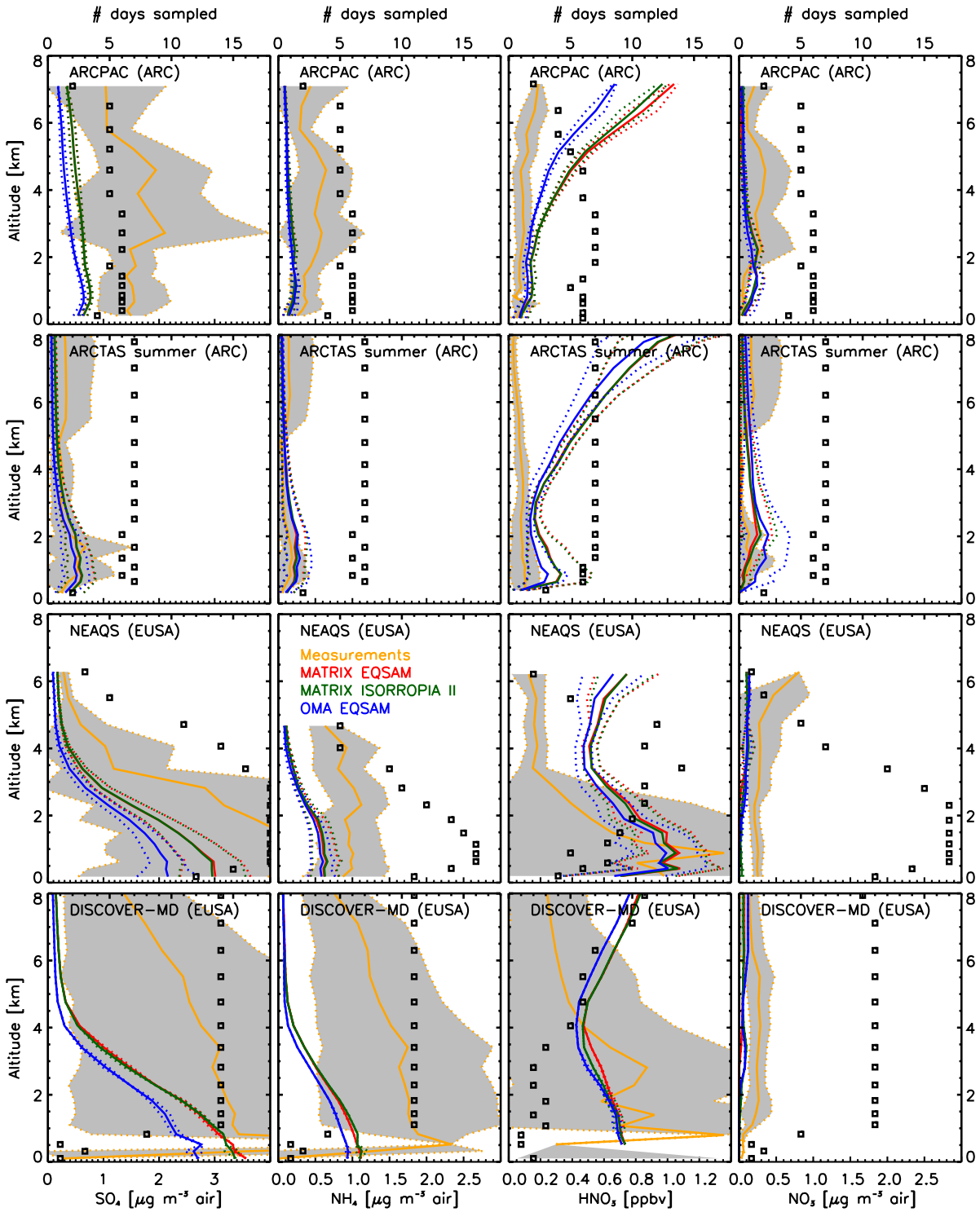

802

803 **Figure A2.** Mean regional concentration profiles. First column is SO_4, second is NH_4, third is
804 HNO_3 and fourth is NO_3. Measurements are in orange, MATRIX-EQSAM is in red, MATRIX-
805 ISORROPIA II is in green and OMA-EQSAM is in blue.

806

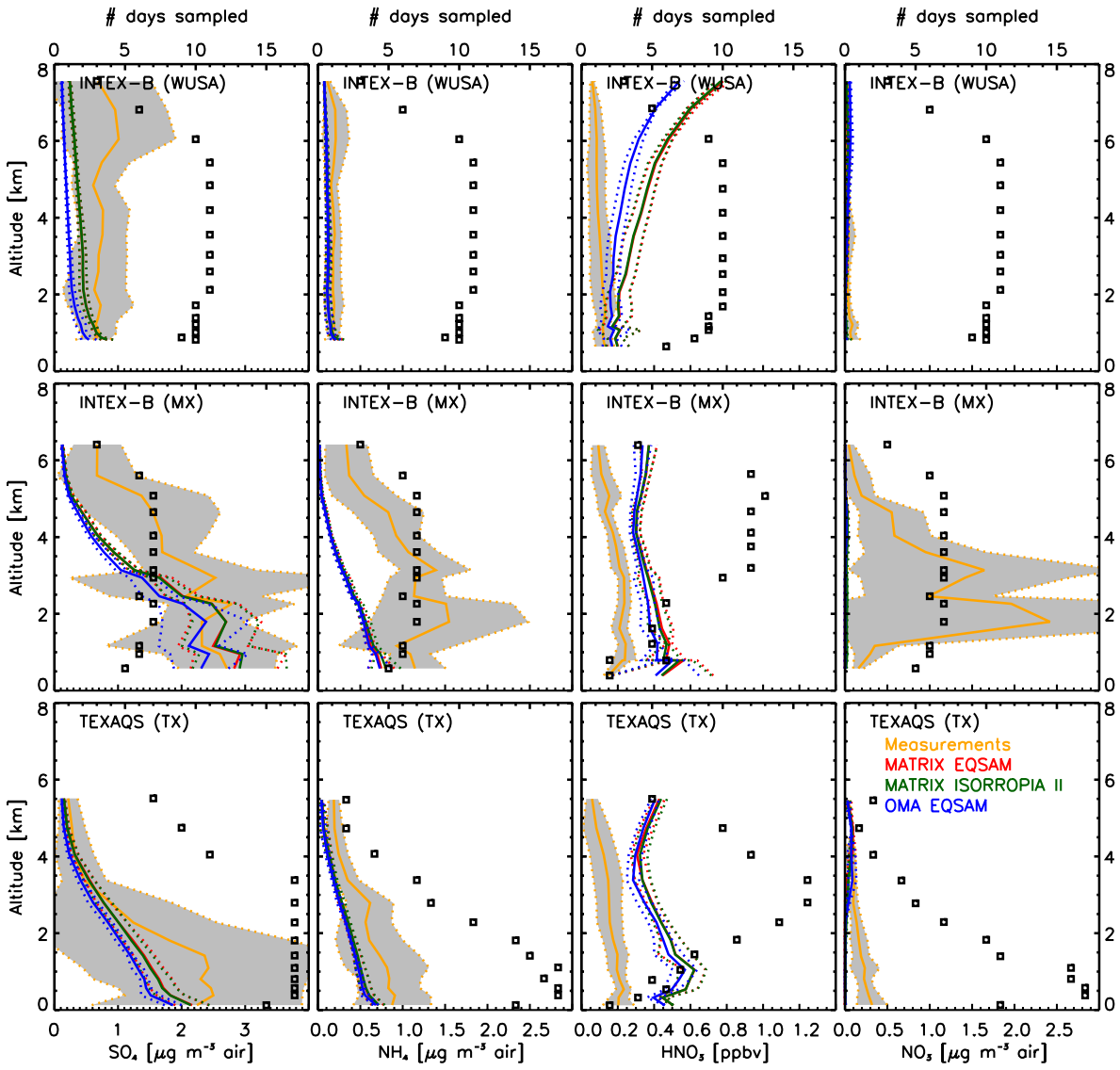

807

808 **Figure A2**: continued

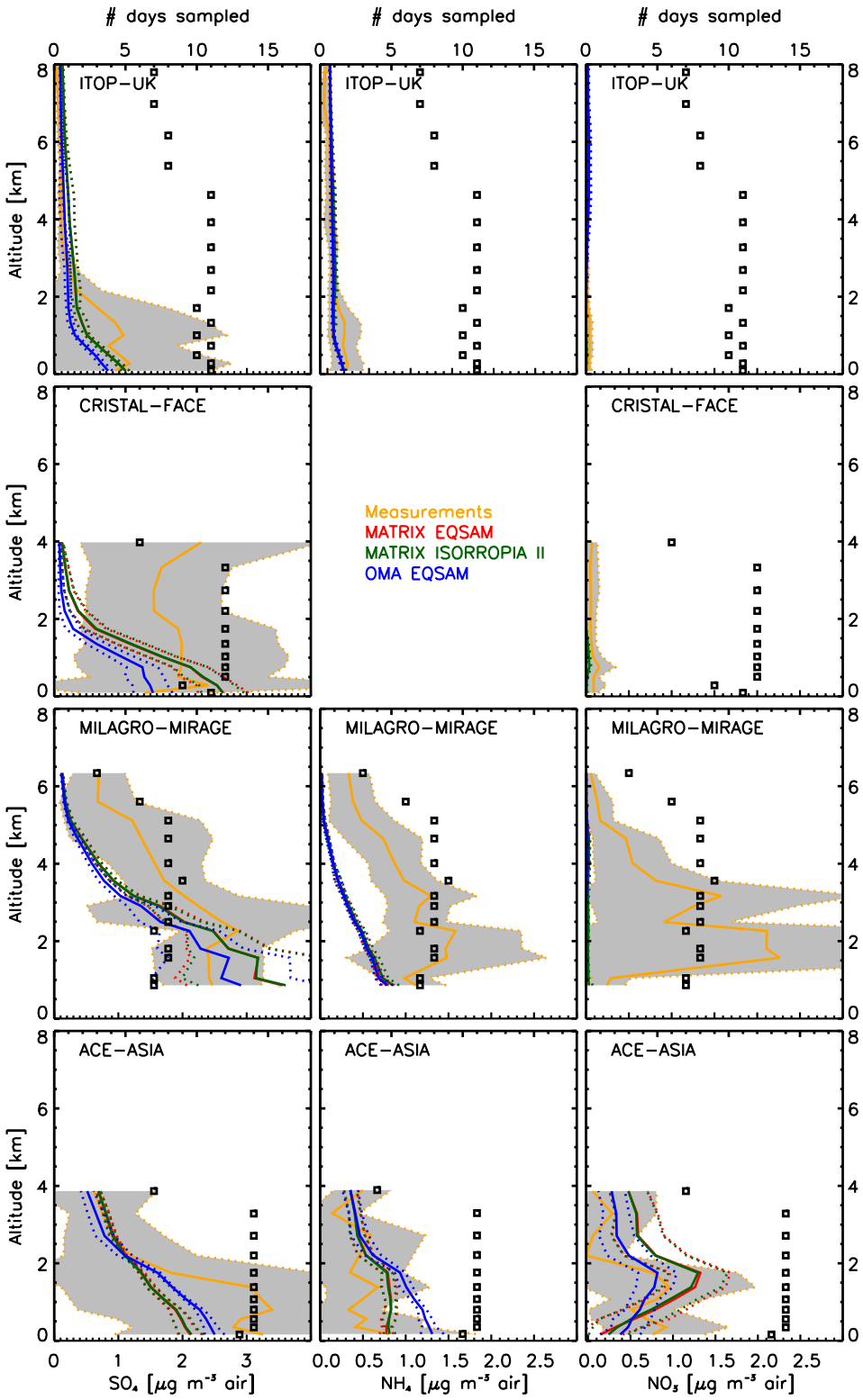

809

810 **Figure A3.** Mean regional concentration profiles. First column is SO_4, second is NH_4, and third is
811 NO_3. Measurements are in orange, MATRIX-EQSAM is in red, MATRIX-ISORROPIA II is in green
812 and OMA-EQSAM is in blue.

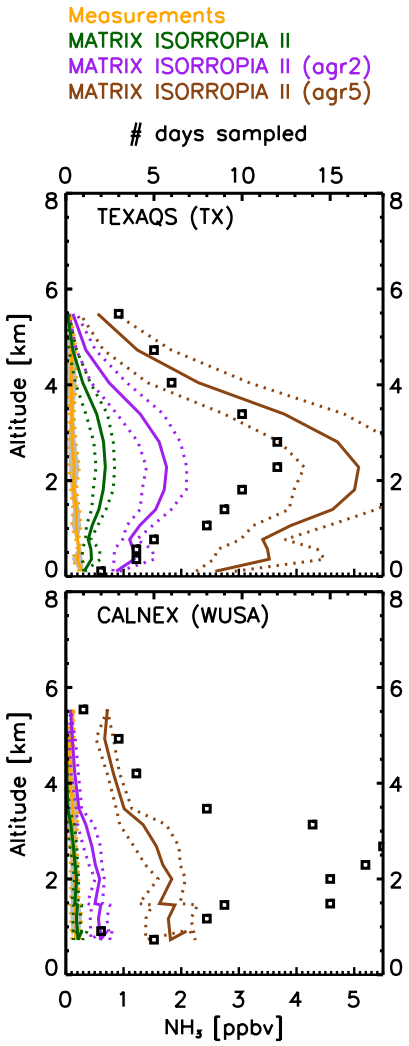

813

814 **Figure A4.** Mean regional NH_3 profiles from the TexAQS (upper panel) and CALNEX (lower
815 panel) campaigns. Measurements are in orange, MATRIX-ISORROPIA II: with regular emissions
816 is in green, with double agricultural NH_3 emissions is in purple, and with 5-times agricultural
817 NH_3 emissions is in brown.

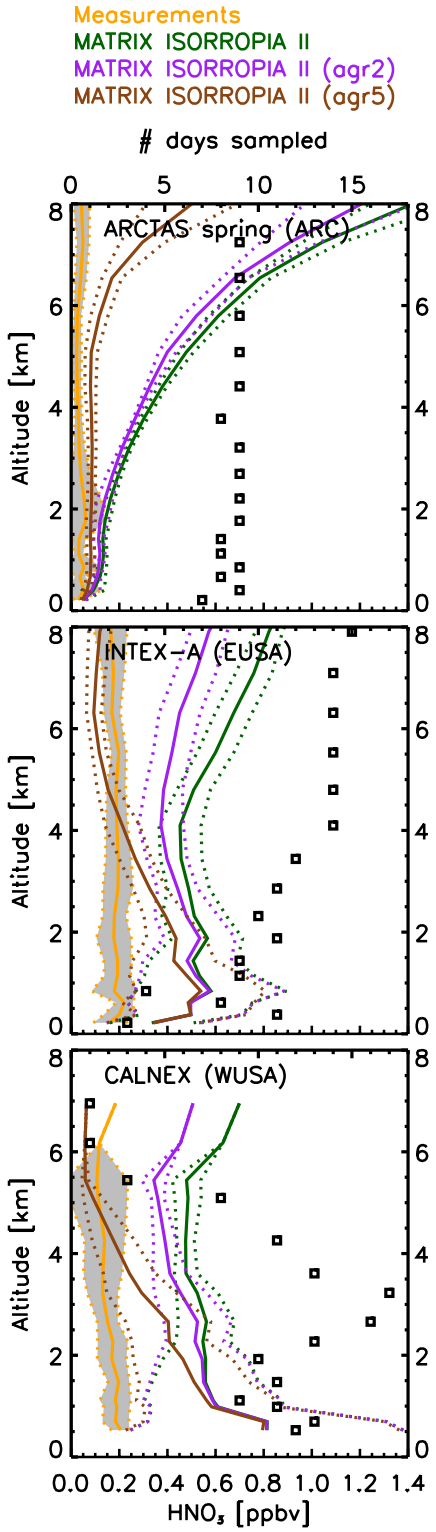

818

819 **Figure A5.** Mean regional HNO_3 profiles from the arctic, EUSA and WUSA. Measurements are in
820 orange, MATRIX-ISORROPIA II: with regular emissions is in green, with double agricultural NH_3
821 emissions is in purple, and with 5-times agricultural NH_3 emissions is in brown.